Clinical and Translational Radiation Oncology 49 (2024) 100860

Contents lists available at ScienceDirect

Clinical and Translational Radiation Oncology

journal homepage: www.sciencedirect.com/journal/clinical-and-translational-radiation-oncology

Review Article

The oxygen puzzle in FLASH radiotherapy: A comprehensive review and experimental outlook

Andrea Scarmelotto [a,1], Victor Delprat [a,1], Carine Michiels [b,2], Stéphane Lucas [a,c,2], Anne-Catherine Heuskin [a,2,*]

[a] Laboratory for Analysis by Nuclear Reaction (LARN), Namur Research Institute for Life Sciences (NARILIS), University of Namur, Rue de Bruxelles 61, B-5000 Namur, Belgium

[b] Unité de Recherche en Biologie Cellulaire (URBC), Namur Research Institute For Life Sciences (NARILIS), University of Namur, Rue de Bruxelles 61, B-5000 Namur, Belgium

[c] Ion Beam Application (IBA), Chemin du Cyclotron, 6, B-1348 Louvain-La-Neuve, Belgium

ARTICLE INFO

Keywords:
FLASH RT
UHDR
ROS
Particle therapy
LET
Ferroptosis
Lipid peroxidation
Ionizing radiation
Preclinical studies
Hypoxia

ABSTRACT

FLASH radiotherapy is attracting increasing interest because it maintains tumor control while inflicting less damage to normal tissues compared to conventional radiotherapy. This sparing effect, the so-called FLASH effect, is achieved when radiation is delivered at ultra-high dose rates (≥40 Gy/s). Although the FLASH effect has already been demonstrated in several preclinical models, a complete mechanistic description explaining why tumors and normal tissues respond differently is still missing. None of the current hypotheses fully explains the experimental evidence. A common point between many of these is the role of oxygen, which is described as a major factor, either through transient hypoxia in the form of dissolved molecules, or reactive oxygen species (ROS). Therefore, this review focuses on both forms of this molecule, retracing old and more recent theories, while proposing new mechanisms that could provide a complete description of the FLASH effect based on preclinical and experimental evidence. In addition, this manuscript describes a set of experiments designed to provide the FLASH community with new tools for exploring the post-irradiation fate of ROS and their potential biological implications.

1. Introduction

Radiotherapy (RT) is a frequently used treatment modality in the cure of cancer, with almost 50 % of cancer patients receiving ionizing radiation (IR) worldwide. However, this technique is not exempt from side effects, the main one being damage to healthy tissues surrounding the neoplastic area. This radiation-induced toxicity is the main disadvantage of RT and greatly limits the dose that can be delivered to the tumor, as defined in clinical irradiation planning. Despite improvements aimed at widening the therapeutic window, such as intensity-modulated RT (IMRT), stereotactic RT, spatially fractionated RT, and combination therapies, new treatments are still required [1–4] to permit dose escalation, with more significant tumor control, while simultaneously limiting side effects and improving the patient's quality of life.

Between the 1960s and 1980s, several groups observed a sparing effect on normal tissues after irradiation at high dose rates in *in vitro* and *in vivo* models, without testing the impact of high dose rates on tumor growth [5–8]. In 2014, Favaudon et al. observed that in addition to lower toxicity in normal tissues, ultra-high dose rate (UHDR) irradiation was characterized by the same tumor control as the conventional dose rate (CONV), and they coined the term FLASH effect [9]. According to the current understanding, the FLASH effect can be achieved by limiting the irradiation time to fractions of a second (reaching the millisecond, and sometimes even the microsecond range), thereby drastically increasing the radiation dose rate when compared to the dose rates currently used in clinics (order of hundredths of Gy/s). Despite the lack of a clear "recipe" to induce the FLASH effect, experimental evidence indicates that the sparing effect is triggered by a minimal average dose rate of 40 Gy/s [10], although others suggest a maximal protection observed when the dose rate is above 100 Gy/s [11,12]. However, the

* Corresponding author.
E-mail address: anne-catherine.heuskin@unamur.be (A.-C. Heuskin).
[1] These authors contributed equally.
[2] Co-senior authors.

https://doi.org/10.1016/j.ctro.2024.100860
Received 21 May 2024; Received in revised form 5 September 2024; Accepted 10 September 2024
Available online 18 September 2024

average dose rate does not seem to be the only key parameter triggering the FLASH effect. Recent findings suggest that the dose per pulse (DPP) and dose rate per pulse are equally important, with a combination of UHDR and high DPP (>4 Gy) offering the greatest protection against the cytotoxic effects of IR [13]. In this context, an exhaustive description of the (frequently omitted) irradiation parameters used in each study — instantaneous dose rate, DPP, pulse frequency, mean dose rate, overall irradiation time, and radiation linear energy transfer (LET) — would allow a clearer definition of the physical conditions required to trigger the FLASH effect [14–16].

To date, the "FLASH effect" has been mainly studied in mice (tumor-free and tumor-bearing) [10], but also in large mammals such as mini-pigs [17,18], cats [17,18] dogs [19,20], humans [21,22], but also zebrafish [23–25] and *C. elegans* embryos [26,27]. Table 1 summarizes the investigations focusing on the outcome of UHDR irradiation in normal tissues, independent of the radiation type. Table 2 summarizes the results of *in vitro* investigations, showing the impact of UHDR irradiation on both normal and cancer cells. Despite the diversity of the irradiated targets, most of these investigations share a low to medium LET (reaching a maximum of few tens of keV/μm in water in some cases [28,29]). To date, only a few studies have been conducted on medium- or high-LET. It would be interesting to swipe over the LET range with the same biological endpoint to study whether the FLASH effect is affected by the beam ionization density. In addition, the O_2 concentration has a crucial impact on triggering a differential biological response between CONV and UHDR irradiation.

However, a complete mechanistic description of the FLASH phenomenon is currently lacking. Oxygen tension in the irradiated tissue plays a prominent role in the occurrence of the FLASH effect, as highlighted in both *in vivo* [26,62] and *in vitro* studies [48]. Indeed, *in vivo*, the sparing effect in the brains of mice after UHDR irradiation was reversed by increased oxygenation obtained through carbogen breathing [26], or when high levels of oxygen were used as carriers for the administration of anesthetic gas to the skin and brain of mice [63,64]. These observations were further confirmed in the skin of mice, where the sparing effect was impaired by the modification (either an increase or decrease) of the oxygen concentration in the irradiated area [65]. Interestingly, while the modification of oxygen tension was shown to abrogate the normal tissue-protective effect offered by UHDR irradiation, it was shown to be as effective in controlling the growth of acute hypoxic tumors as it is for physiological tumors [66]. Indeed, although a decrease in oxygen concentration during irradiation induced a strong decrease in tumor control after CONV irradiation [66,67], UHDR irradiation was not affected by acute hypoxia. *In vitro,* however, the role of oxygen is not straightforward, as shown in, where four out of seven cancer cell lines showed higher surviving fractions after UHDR irradiation under normoxic conditions (21 % O_2), suggesting that a reduced O_2 concentration may not be a universal requirement for triggering the FLASH effect *in vitro*.

Because of the significant impact of oxygen tension on the occurrence of the FLASH effect, this review describes several hypotheses related to oxygen, either as dissolved molecules or reactive oxygen species (ROS). Section 2 discusses the rise and fall of the oxygen depletion hypothesis. In Section 3, *in silico, in vitro*, and *in vivo* studies investigating ROS production following UHDR and CONV irradiation are described. The importance of investigating ROS production (either directly or indirectly) following UHDR and CONV irradiation is also highlighted, and, in Section 4, a few approaches aiming to experimentally determine ROS production *in vivo* upon UHDR and CONV irradiation are proposed. The production of ROS and their impact on cellular damage, such as ferroptosis, mitochondrial damage, and senescence/inflammation, are described in Section 5. This ROS-induced cellular damage may provide new insights into the differential effects observed in normal tissues compared to those in tumors upon UHDR irradiation. Finally, we propose a hypothetical model that could be involved in the FLASH effect, based on differential ROS production (caused by different oxygen tensions between the two tissues) and cellular differences (including a higher labile iron pool in cancer cells than in normal cells) between normal and tumor tissues.

2. O_2 depletion cannot be the core explanation for the FLASH effect

Oxygen also plays a pivotal role in the DNA response to IR and is the main actor in what is called oxygen fixation theory. Most radiation-induced DNA damage is efficiently repaired by an endogenous DNA damage response (DDR). However, this task is prevented when O_2 reacts with DNA radicals to produce peroxyl radicals, $RO_2^{\bullet}$, whose repair through DDR is difficult or impossible [68,69]. The oxygen fixation theory is one of the most important concepts in radiobiology and is one of the main theories explaining the higher radioresistance of hypoxic cells. Hence, a decrease in O_2 concentration is associated with radioprotection owing to reduced DNA damage. Tumor hypoxia is a key feature of the tumor microenvironment and has a strong impact on tumor initiation, progression, and metastasis [70–72]. Hence, tumor hypoxia is primarily associated with poor prognosis after RT [73]. Hypoxia induces complex cell reprogramming mostly by activating hypoxia-inducible factors (HIFs) [74]. HIFs are transcription factors, composed of an α-subunit stabilized specifically under hypoxia and a β-subunit constitutively expressed. Three α-subunits exist (HIF1α, HIF2α, and HIF3α), and the one most often described is HIF1α [75]. Accordingly, high HIF1α and/or HIF2α expression in tumors is mostly associated with poor prognosis and with a poor response following RT [72]. Furthermore, HIF1α activation is associated with a strong radioprotection. Indeed, the silencing of HIF1α is associated with an increase in RT sensitivity, both *in vitro* and *in vivo*, likely via resistance to apoptosis induction, metabolism modification (increase of glycolysis metabolism), and cell cycle regulation (cell cycle arrest) [74]. In conclusion, severe hypoxia is associated with cell radioresistance via reduced DNA damage fixation (the oxygen fixation theory) and the induction of cell reprogramming, which is mostly mediated by HIF transcription factors.

The depletion of oxygen was the first hypothesis to explain the FLASH sparing effect observed in normal tissues, according to which, radiochemical oxygen depletion (ROD) at UHDR irradiation would be faster than the time required to reoxygenate the irradiated tissues [76], creating a transient hypoxic (and therefore, radioresistant) region. The basis of this hypothesis traces back to the late 1950s, when Dewey et al. showed a correlation between dose rate and oxygen consumption [77]. However, oxygen depletion increases radioresistance in both normal and tumor tissues [69]. The difference in oxygenation status between cancerous and normal tissues was proposed to be the driving force of the FLASH effect. Indeed, the decrease in O_2 concentration is more pronounced in normal tissues than in neoplastic tissues, making the former relatively more radioresistant. In contrast, a decrease in O_2 concentration would be less relevant in tumors because these tissues are already in severe hypoxia, resulting in no or only a small increase in radioresistance [78,79].

In recent years, the oxygen depletion theory has been challenged several times. *In silico* models have mostly shown that oxygen depletion at UHDR irradiation is negligible in normal tissues at clinically relevant doses and cannot fully explain the increase in radioresistance [80,81].

Experimental measurements of ROD in water phantoms suggest a higher oxygen depletion at CONV irradiation compared to UHDR irradiation, with the former depleting more O_2 than UHDR irradiation for the same dose [82–88]. Interestingly, dose-escalation studies showed that the O_2 depletion per unit dose decreased as the total delivered dose increased, probably owing to the competing recombination of radicals [82,85].

These observations were partially confirmed by oxygen depletion measurements in *in vivo* models. In this context, irradiation of mice showed no O_2 depletion in the CONV group, presumably because ROD is

Table 1
Table 1: list of investigations delivering irradiation at UHDR on in vivo models.

Targeted organ	Biological outcome	Particle used	LET (keV/um) in water	Number of pulses	Pulse width	Pulse dose rate (or Instantaneous dose rate) [Gy/s]	Total dose delivered [Gy]	Dose per pulse [Gy]	Average dose rate [Gy/s]	Total time of irradiation	Ref.
Brain (mice)	FLASH group did not develop neurocognitive deficit. Carbogen breathing annihilates the sparing effect. Lower level of H2O2 (water phantom)	electrons (5.6 MeV)	0.2	1	1.8 μs	5.5 E06	10, 12, 14	10, 12, 14	5.5 E06	1.8 μs	[26]
	UHDR/CONV has same tumor control, with UHDR better preserving cognitive functions at moderate doses	electrons (5.6 MeV)	0.2	1 2 4 3 2	1.8 μs	5.6 E06, 7.8 E06 1.9 E06 3.9 E06 5.6 E06 6.9 E06	10, 14 2 x 7 Gy 4 x 3.5 Gy 3 x 10 Gy 25	10, 14 7 3.5 10 12.5	5.6 E06, 7.8 E06 1.9 E06 3.9 E06 5.6 E06 2.5 E03	1.8 μs each fraction delivered in several days (1,8 μs pulse each day) 10 ms	[30]
	UHDR induced lower inflammation and an ameliorated radiation-induced increases in astrogliosis and microgliosis over early (2–6 weeks) to delayed (6 months) times postirradiation	electrons (5.6 MeV)	0.2	1	1.8 μs	5.5 E06	10	10	5.5 E06	1.8 μs	[31]
	Preservation of cognitive function after 10 Gy WBI single dose after 2 and 6 months PI. Moreover, reduced induction of reactive astrogliosis and preserved hippocampal cell division	X-ray (6 GeV)		1 per slice	270 ms	1.2 E04	10	10	37	270 ms	[32]
	10 Gy WBI showed full memory preservation for dose rate > 100 Gy/s and a gradual descrease of cognitive function as dose rate is lowered (2 months PI)	electrons (5.6 MeV)	0.2	from 1 to 1000	1.8 μs	5.5 E06	10	10	from 5.5 E06 to 0.1 Gy/s	from 1.8 μs to 100 s	[17]
	Reduced memory impairment and no significant reduction of dendritic spine density for UHDR cohort. At UHDR, fewer inflammation markers were overexpressed (3 at UHDR, 5 in CONV)	electrons (16 and 20 MeV)	around 0.23	18 pulses on average	2 μs	8.75 E05	30	1.75	200 and 300 Gy/s	0.1 s (for 300 Gy/s) or 0.16 (for 200 Gy/s)	[33]
	UHDR is better in preserving hippocampal and	electrons (6 MeV)	0.2	1	1.8 μs	4.4 E06	8	8	4.4 E06	1.8 μs	[34]

(*continued on next page*)

Table 1 (*continued*)

Targeted organ	Biological outcome	Particle used	LET (keV/um) in water	Number of pulses	Pulse width	Pulse dose rate (or Instantaneous dose rate) [Gy/s]	Total dose delivered [Gy]	Dose per pulse [Gy]	Average dose rate [Gy/s]	Total time of irradiation	Ref.
	perirhinal cortical circuity, without anxiety/depression, and social interaction comparable with CTR										
	UHDR had lower impact on vasculature, higher expression of junction protein, and without inducing apoptosis (24 h and 1 week PI at 25 Gy)	electrons (5.6 MeV)	0.2	2	1.8 μs	6.9 E06	25	12.5	2500	10 ms	[35]
Lung	No lung fibrosis up to 20 Gy in FLASH; 30 Gy FLASH and 7.5 Gy CONV activated caspase-3 to a similar extent	electrons (4,5 MeV)	0.2	not provided	1 μs	not provided	17, 20 and 30	17, 20 and 30	60	from 283 to 500 ms	[9]
	Alveolar structure of FLASH cohort was similar to CTR (while alveolar fibrosis in CONV was more severe)	X-ray (8 MeV)	/	1	25 ms	1200	30	30	1200	25 ms	[36]
Abdomen (mice)	Higher LD50 for mice irradiated at UHDR	protons (230 MeV)	0.4	from 80 to 150	21 μs	6200	From 10 to 19	0.125	96	from 100 to 200 ms	[37]
	UHDR group had more remaining crypts and lower alteration between 7.5 and 12 Gy. A reduction of the average dose rate (increasing the number of pulses/increasing time between pulses) resulted in lower crypt survival	electrons (6 MeV)	0.2	From 1 to 1250 pulses	3.4 μs	From 3.3 E06 to 1.1 E04	From 0 to 20 Gy (crypts survival) 12 Gy (impact of beam structure)	From 0.01 to 20 Gy	From 0.25 to 3.3 E06	From 3.4 μs to 30 s	[38]
	In tumor-free mice, UHDR showed higer surviving fraction, and a 2-fold higher presence of regenerating crypts. No differences in hemotopoietic toxicity (16 Gy). UHDR group had higher epithelial integrity and, overall, less radiation-induced intestinal injury than CONV group	electrons (16 MeV)	0.23	7 or 8	5 μs	4 E05	14 or 16 Gy	2	216	80 ms	[39]
	UHDR/CONV had same tumor control. In tumor-	proton (230 MeV)	2–3 (SOBP),	1	140 μs	108	15	15	108	140 ms	[40]

(*continued on next page*)

Table 1 (*continued*)

Targeted organ	Biological outcome	Particle used	LET (keV/um) in water	Number of pulses	Pulse width	Pulse dose rate (or Instantaneous dose rate) [Gy/s]	Total dose delivered [Gy]	Dose per pulse [Gy]	Average dose rate [Gy/s]	Total time of irradiation	Ref.
	free mice, significantly higher number of regenerating crypts after SOBP/plateau UDHR compared to CONV		0.4 (plateau)								
	CONV depleted less circulating bodies and lymphocytes than UHDR. In addition, higher surviving fraction after 16 Gy gastric irradiation at CONV compared to UHDR	electrons (20 MeV)	0.24	not measured	4 μs	not measured	16	not measured	35	450 ms	[41]
	UHDR preserved proliferating crypts and induced less fibrosis than CONV, maintaining same tumor control	proton (230 MeV)	0.4 (plateau)	1	approx. 0.2 s	78	15 or 18 Gy	15 or 18 Gy	78	approx. 0.2 s	[42]
Nasal (cat)	Low skin toxicity at > 12 months PI with local tumor control for 5 out of 6 cats	electrons (5.6 MeV)	0.2	not provided	not provided	5 E06	from 25 to 41	from 25 to 41	300	from 80 to 130 ms	[17]
Skin (mice)	Less skin toxicity at UHDR vs CONV for doses > 30 Gy	electrons (16 MeV)	0.23	5, 8, 10, 15, 20	5 μs	4.0 E05	10, 16, 20, 30, 40	2	180	from 55 to 222 ms	[43]
Skin (mini-pig)	FLASH spots histologically comparable to CTR, with no skin alteration and hair follicle preservation only at UHDR	electrons (5.6 MeV)	0.2	not provided	not provided	5 E06	from 22 to 34	from 22 to 34	300	from 70 to 100 ms	[17]
Skin (human, cutaneous lymphoma)	Single fraction at UHDR resulted in less side effects than previous fractionated treatments (20 Gy in 10 fractions, or 21 Gy in 6 fractions), maintaining the efficacy against the tumor	electrons (5.6 MeV)	0.2	10	1 μs	E06	15	1.5	166	90 ms	[21,22]
Zebrafish embryo	UHDR embryos were significantly longer than CONV group for doses > 10 Gy	electrons (5.6 MeV)	0.2	not provided	not provided	> 1.8 E05	from 5 to 12	not provided	> 40	< 200 ms	[44]
	Higher surviving fraction after CONV vs UHDR, despite showing	electrons (20 MeV)	0.24	1441	5 ps	E09	26	0.018	2.4 E05	111 μs	[45]

(*continued on next page*)

Table 1 (*continued*)

Targeted organ	Biological outcome	Particle used	LET (keV/um) in water	Number of pulses	Pulse width	Pulse dose rate (or Instantaneous dose rate) [Gy/s]	Total dose delivered [Gy]	Dose per pulse [Gy]	Average dose rate [Gy/s]	Total time of irradiation	Ref.
	less morphological alterations										
	Comparable embryonic survival or structural integrity after UHDR vs CONV	proton (224 MeV)	0.41	single pulse	single pulse	500	from 10 to 42.5	not provided	100	from 100 to 420 ms	[46]
	Higher body length after UHDR irradiation compared to CONV 4 days post-irradiation, while no differences in survival or spinal curvature were observed	proton (68 MeV)	0.97	single pulse	< 5 ms	> 8 E03	30 or 40 Gy	30 or 40 Gy	> 8 E03	< 5 ms	[47]
C. elegans	Lower growth delay after UHDR irradiation compared to CONV	proton (4 Mev) and electron (9 MeV)	10 for proton, 0.2 for electron	1 pulse for proton, 8 or 16 for electron	10 and 20 ms for protons, 77 or 165 ms for electron	1000 Gy/s for proton, 6.6 E05 for electron	10 and 20 Gy	10 or 20 Gy for proton, 1.3 for electron	1000 Gy/s for proton, 126 Gy/s for electron	10 and 20 ms for protons, 77 or 165 ms for electron	[27]

slower than oxygen rediffusion from the vascular system. At the same time, a slight decrease in tissue oxygen concentration could be detected at UHDR irradiation, both with proton and electron beams, which was more pronounced in oxygenated normal tissues than in hypoxic tumors [84,85]. In conclusion, despite the small transient decrease in oxygen concentration induced by UHDR irradiation, a large body of literature agrees on considering ROD as one of the contributors to the FLASH effect rather than the main driving force.

Molecular oxygen is the main factor in the fixation of IR-induced DNA damage and represents the most important cause of cell death, regardless of the dose rate. Surprisingly, no study so far has showed that DNA damage can account, on its own, for the observation of the FLASH effect. Indeed, although some studies reported lower DNA foci numbers after UHDR irradiation for doses >20 Gy [54,89] and for early time points only [52], other studies showed no significant difference in DNA damage induction (at least for double-strand breaks (DSBs)) when the two irradiation regimes were compared [10,49,90–92]. To date, only a few studies on DNA damage with exposure to moderate LET have been published [27,28]. Investigating the DDR of high-LET UHDR irradiation could provide valuable insights for determining the specific impact of the DNA response on the FLASH effect. This could be done by assessing, for example, if (and eventually, how) high-LET radiations in the UHDR regime impact the nature and/or efficiency of DNA repair mechanisms, or if they could activate specific DDR pathways not triggered by CONV irradiation. In conclusion, while the role of DNA damage in the FLASH effect is still uncertain, it is well established that IR-induced oxygen depletion is only one of several contributors to this phenomenon.

3. Reactive oxygen species at UHDR and CONV RT

3.1. Simulation

In common clinical practice, IR is delivered at a dose rate on the order of a few Gy/min. The resulting ionization tracks are well-separated over time and are therefore thought to be independent of each other. In such configurations, interactions between radical species originating from different tracks are unlikely.

However, upon UHDR irradiation, the tracks are much less separated in time owing to the very short timeframe required to perform irradiation, ranging from micro- to milliseconds. Therefore, intertrack interactions are more likely and must be considered, because the time required to deliver the radiation dose is comparable to the temporal lifespan of the radical species [93]. Recombination between tracks can modify the yield of radiolytic products and their biological effects on the cell.

Thompson et al. investigated how the probability of interaction between tracks changes according to the energy of the particle. Proton simulations were performed using the TOPAS toolkit, and different timeframes ranging from 1 ps to 1 ns were investigated. Their study confirmed that the intertrack probability is low when clinically relevant doses are considered, and become relevant only for doses above 20 Gy for high-energy, low-LET protons (even higher doses are required for higher-LET protons). In addition, the impact of intertrack interactions on the radiolytic yield of chemical species was studied for protons of different LETs. No significant differences were observed in the molecular yield of hydrogen peroxide species, for biologically relevant timeframes within a clinically relevant dose range [94]. This observation was confirmed by Alanazi et al., who simulated the impact of dose and dose rate on the modification of radiolytic yield. More precisely, the authors reported a significant increase in molecular yield exclusively with sparsely ionizing high energy, low-LET protons (300 MeV, LET of 0.3 keV/μm) and doses above 70 Gy [95].

Kreipl et al. [96] exploited the PARTRAC code to investigate the production of hydroxyl radicals, starting from 1 ps after radiation until the end of the heterogeneous chemical phase (approximately 1 μs). The authors, considering 20 MeV protons, predicted that only high doses (> 50 Gy) could impact the yield of $OH^{\bullet}$ radicals, in agreement with Thompson et al., who further investigated the probability of intertrack interactions and consequent modification of the radical yield for proton beams of different LETs [94].

Table 2
.Table 2: list of investigations delivering irradiation at UHDR on in vitro models

Cell line	Biological outcome	Particle used	LET (keV/um) in water	Number of pulses	Pulse width	Pulse dose rate [Gy/s]	Total dose delivered [Gy]	Dose per pulse [Gy]	Average dose rate [Gy/s]	Oxygen concentration	Total time of irradiation	Ref.
DU 145 (prostate cancer cell line)	**Clonogenic assay (from 1.6 % O2 to normoxia)**: no FLASH in normoxic condition; sparing effect in hypoxia (1,6% O2) for dose > 15 Gy	electrons (10 MeV)	0.21	from 1 to 7	3,5 μs	From 8,6 E06 Gy/s (single pulse) to 714 Gy/s (8 pulses)	from 3 to 25 Gy, in multiples of 3 Gy	3	600	1.6–2.7–4.4–8.3–20 % O2	From 3,5 μs (single pulse) to 35 ms (8 pulses)	[48]
MCF7, MDA-MB-231 (human breast cancer), HeLa, LU-HNSCC4 (SCC from patient), WiDr (colon cancer). MRC5 (human fibroblast)	A trend of increased surviving fraction after UHDR irradiation (**clonogenic assay**). DNA-foci formation (**53BP1**) and cell synchronization gave similar responses after UHDR or CONV irradiatio1)	electrons (10 MeV)	0.21	from 1 to 4	3,5 μs	8.6 E05	from 3 to 12 Gy, in multiples of 3 Gy	3	From 800 Gy/s (4 pulses) to 8,6 E05 (single pulse)	normoxia	From 3,5 μs (single pulse) to 15 ms (4 pulses)	[49]
A549 (lung cancer) vsIMR90 (normal lung fibroblast)	FLASH significantly reduces viability in cancer cells, but not normal cells (**clonogenic assay + CCK-8**). Limited damage to mitohondria of normal cells. Lower radiolytic yield of H2O2 at UHDR vs CONV (**water phantom**)	proton (4,5 MeV)	10	1	From 15 ms (1,5 Gy) to 150 ms (15 Gy)	100	From 1,5 to 15 Gy	From 1,5 to 15 Gy	100	normoxia	From 15 ms (1,5 Gy) to 150 ms (15 Gy)	[50]
A549 and H1437	No difference was observed at normoxic condition (**clonogenic assay** and in **RIF number**); the sparing effect was observed ONLY at FLASH dose rate, low O2 tension and for doses > 8 Gy.	He ions	4,5 at Pristine Bragg peak, 16 in SOBP	1	From 14 to 86 ms	from 140 to 210	From 2 to 12 Gy	From 2 to 12 Gy	from 140 to 210	normoxia and 1 % O2	from 14 ms (2 Gy) to 86 ms (12 Gy)	[51]
PBMCs (human peripherial blood mononuclear cells)	UHDR as potent as CONV in killing ex-vivo PBMCs. Same was observed with in-vivo circulating lymphocytes	electrons (20 MeV)	0.24	several	4	not measured	Dose escalation (0, 2, 4, 6, 8 Gy) for clonogenic assay; Single dose (2 Gy) to assess apoptosis in PBMCs	not measured	35	normoxia	From 60 (2 Gy) to 200 ms (8 Gy)	[41]
KPC and Panc02 (both murine pancreatic cell lines)	**Clonogenic assay**: UHDR is more potent in reducing cell clonogenicity than CONV											
H454 (murine glioblastoma)	**Clonogenic assay**: UHDR and CONV were isotoxic at 10 Gy in reducing cell, whereas higher surviving fraction at 20 Gy UHDR (3-fold increase in normoxia, 6-fold increase at 4 % O2)	electrons (5,6 MeV)	0.2	2 or 3	approx. 0.2 μs	1,8 E06	10 or 20 Gy	5 or 6,6 Gy	100	normoxia and physioxia (4 % O2)	From 100 (10 Gy) to 200 ms (20 Gy)	[26]
MRC5, IMR90 (healthy lung), PBEC (primary bronchial ephitelial cells), A549 (cancer lung)	**DNA damage (53BP1, g-H2AX; 30 min PI)**: significant lower 53BP1 foci number after UHDR irradiation for both normal cell lines. Conversely, no difference was observed for A549 (5 Gy).UHDR spares	electrons (4,5 MeV)	0.2	from 3 (2 Gy) to 7 (5 Gy)	1,45 μs	4,6 E05	5 Gy for DNA damage, 2 or 4 Gy to assess proliferation and differentiation in PBEC	0.7	75	normoxia	From 30 (2 Gy) to 70 ms (5 Gy)	[52]

(*continued on next page*)

Table 2 (*continued*)

Cell line	Biological outcome	Particle used	LET (keV/um) in water	Number of pulses	Pulse width	Pulse dose rate [Gy/s]	Total dose delivered [Gy]	Dose per pulse [Gy]	Average dose rate [Gy/s]	Oxygen concentration	Total time of irradiation	Ref.
	PBEC from radiation-induced cell death for moderate doses of radiation (4 Gy)											
A549 spheroids.HT-26, MDA-MB-321 for confirmation (SPHEROIDS)	**Growth assay:** higher clonogenic survival for irradiation at UHDR compared to CONV for spheroids model until 15 Gy. No difference was observed for monolayer using the same beam parameter	electrons (16 MeV)	0.23	5, 10, 15, 20	5 μs	4 E05	5, 10, 15, 20	1	90	oxygen gradient (intrinsic property of spheroid)	from 50 (5 Gy) to 200 ms (20 Gy)	[53]
IMR90 (normal lung fibroblast)	**Clonogenic assay**: no statistically difference in surv. fraction at any tested doses (indipendently on dose rate). **DNA damage (g-H2AX, 30 min PI)**: lower RIF number for highest dose (20 Gy) at highest dose rate (1000 Gy/s). **Senescence induction (b-gal, 2 months PI)**: lower induction of senescence for 100 and 1000 Gy/s vs CONV (20 Gy). **TGF-beta expression**: lower expression of TGF after irradiation at 1000 Gy/s vs CONV (assessment made only at 20 Gy)	proton (4,5 MeV)	10	1	< 100 ms for clonogenic assay and DNA IRIF formation; < 200 ms for senescence and TGF expression	100 or 1000	From 0,5 to 20 Gy	From 0,5 to 20 Gy	100 or 1000	normoxia	< 100 ms for clonogenic assay and DNA IRIF formation; < 200 ms for senescence and TGF expression	[54]
Mammalian cells (HeLa S.3 cells)	**Clonogenic assay (no comparison with CONV):** higher surviving fraction with higher average dose rate, and in hypoxic condition (0.35 % and 0 % vs 21 % O2)	electrons (15 MeV)	0.23	1 or 2	1.3 μs	3.5 E07 for 45 Gy	from 2 to 45 Gy	from 2 to 45 Gy	> E06	Normoxia and hypoxia	1.3 μs (single pulse) or 5.2 μs (two pulses)	[8]
HeLa, P.388 (leukemia cells extracted from murine donor)	**Clonogenic assay (no comparison with CONV):** higher surviving fraction when cells are under hypoxic conditions (0.35 % or 0 % O2)	electrons (400 keV)	0.21	single pulse	3 ns	approx. E9	from 2 to 25 Gy	from 2 to 25 Gy	approx. E9	0 % and 21 % O2	3 ns	[55]
HeLa	**Clonogenic assay (no comparison with CONV):** irradiation in hypoxic (0.35 % O2) or anoxic condition increases cell survival	electron		single pulse	1 μs	from 3 E06 to 2.7 E07	from 3 to 27 Gy	from 3 to 27 Gy	from 3 E06 to 2.7 E07	0, 0.35 and 21 % O2	1 μs	[56]
HeLa	**Clonogenic assay (no comparison with CONV)**: surviving fraction of hypoxic cells (0.35 % O2) is higher than normoxic ones	electrons (10 MeV)	0.21	single pulse	10 ns	2 E07	from 3 to 33 Gy	from 3 to 33 Gy	2 E07	normoxia and hypoxia	10 ns	[57]

(*continued on next page*)

Table 2 (*continued*)

Cell line	Biological outcome	Particle used	LET (keV/um) in water	Number of pulses	Pulse width	Pulse dose rate [Gy/s]	Total dose delivered [Gy]	Dose per pulse [Gy]	Average dose rate [Gy/s]	Oxygen concentration	Total time of irradiation	Ref.
U-87 MG, HT-144, V79	**Clonogenic assay**: no difference in surviving fraction between irradiation at UHDR and CONV, in normoxic and anoxic (<0.02 % O2) condition	electrons (20 MeV)	0.24	single pulse	3.2 μs	from 6 to 30 E08	from 2 to 27 Gy	from 2 to 27 Gy	from 6 to 30 E08	0 and 21 % O2	3.2 μs	[58]
mice fibroblast (V79-379-A)	**Clonogenic assay**: no difference in surviving fraction in normoxia up to 15 Gy, nor in anoxia up to 38 Gy between UHDR and CONV	electrons (50 MeV)	0.32	from 4 to 8 in oxic cond., from 12 to 24 in anoxic cond.	6 μs	2.7 E05	from 3.2 to 38 Gy	1.6 Gy	380	0 and 21 % O2	from 20 to 120 ms	[59]
CHO	**Clonogenic assay**: no difference in surviving fraction between UHDR and CONV.As O2 concentration decreases, surviving fraction of cells irradiated at UHDR increases	electrons (600 keV)	0.19	single pulse	3 ns	approx. E9	from 0 to 50 Gy	from 0 to 50 Gy	approx. E9	0 and 0.5 % O2	3 ns	[60]
HeLa	**Clonogenic assay (no comparison with CONV)**: higher surviving fraction when cells are irradiated at UHDR and kept in hypoxic condition. As O2 level decreases, surviving fraction increases.	electrons (350 keV)	0.22	single pulse	3 ns	not provided	from 0 to 40 Gy	from 0 to 40 Gy	not provided	0 and 1 % O2	3 ns	[5]
HeLa, CHL-F	**Clonogenic assay:** higher surviving fraction after irradiation at UHDR for high doses (>5 Gy)	X-ray (2 MVp or 3.7 MV)		single pulse	few tens of ns	from 0.3 to 2 E09	from 2 to 15 Gy	from 2 to 15 Gy	from 0.3 to 2 E09	normoxia	few tens of ns	[61]

Finally, to study the interaction of primary radiolytic species resulting from water radiolysis, Abolfath et al. performed a molecular dynamics simulation and observed the formation of spaghetti-like agglomerates of ROS, whose mobility and reactivity were mitigated by the presence of intermolecular interactions (such as hydrogen bonds and electric polarity forces) between single radical species. The authors reported that these ROS complexes (called non-ROS) are formed only at UHDR irradiation, and are more likely to be formed under physiological O_2 conditions (4–5 % O_2) than in hypoxic regions [97].

Taken together, these studies agree on attributing only a small impact to the interaction between primary radiolytic radicals at clinically relevant doses, even when the dose rate is increased above the UHDR limit.

3.2. Experimental investigations

Other groups have experimentally investigated the impact of the radiation dose rate on ROS and H_2O_2 production *in vitro*, *in vivo*, and through water phantom irradiation. Guo et al. assessed ROS production in IMR90 cells exposed to proton irradiation at a UHDR (100 Gy/s) or CONV with or without incubation with the ROS scavenger N-acetylcysteine (NAC). This experiment showed a clear difference in terms of ROS production, with UHDR irradiation producing less ROS than CONV irradiation [50]. Consistently, Montay-Gruel et al. showed that NAC and amifostine, two antioxidant molecules, reduced the toxicity of CONV irradiation in zebrafish, whereas they had no effect on UHDR irradiation, suggesting that ROS toxicity and/or production are lower in UHDR irradiation (vs. CONV irradiation) [26]. Of note, neither NAC nor amifostine are specific antioxidants, meaning that it is not possible to gain any insights into the impact of radiation dose rate on the yield of a specific ROS. For this purpose, overexpression of superoxide dismutase 2 (a specific superoxide scavenger) or mitochondrial catalase (a specific H_2O_2 scavenger), which has already been shown to decrease radiation-induced normal tissue injury, could be investigated [98]. In contrast, Kim et al. observed the opposite trend, measuring higher ROS production in UHDR-irradiated tumor tissues using a 2′,7′-dichlorodihydrofluorescein diacetate (DCFDA) fluorescent probe [99], although the detection of ROS in tissue sections using this technique is technically questionable due to the extremely short lifetime of these species [100]. Furthermore, through water phantom irradiation, several groups have reported a negative correlation between the H_2O_2 yield and dose rate [26,87,101], and a more pronounced difference for electrons compared to proton irradiation [102,103]. In addition, ROS production was assessed using the nonspecific ROS sensor CellROX [103]. Generally, ROS production with UHDR irradiation was much lower than that with CONV irradiation (in pure water with both protons and electrons). This decrease in ROS production was more pronounced than that observed with H_2O_2. This suggests that there is also a difference in the yield of ROS other than H_2O_2 (*e.g.,* $OH^{\cdot}$ or superoxide) under UHDR versus CONV irradiation. The lipid peroxidation level, an end product of ROS, was also assessed following proton UHDR and CONV irradiation in a chemical-based model at both 4 % O_2 and 21 % O_2 [104]. The lipid peroxidation level strongly increased in a dose-dependent manner following CONV irradiation, but not following UHDR irradiation. Furthermore, the lipid peroxidation level following CONV irradiation was significantly lower at 4 % O_2 than at 21 % O_2, while the level of lipid ROS after UHDR irradiation was unaffected by varying oxygen levels. We hypothesized that the difference in lipid peroxidation in the CONV versus UHDR regimens would be negligible even at lower oxygen concentrations, mostly relevant to tumor tissue (*i.e.,* below 4 % O_2).

Notably, all water phantom irradiations were performed in pure water at 21 % O_2 [87,101,103] or 4 % O_2 [26,102]. Interestingly, the oxygenation level in normal tissues is generally higher than that in cancer tissues (3.4 %-9.5 % in normal tissues and 0.3 %-2.2 % in cancer) [105,106]. Hence, the studies described above were performed at oxygen concentrations relevant in normal tissues, but not in tumor tissues. Despite the much lower complexity of water phantoms compared to *in vivo* samples, we speculate that UHDR irradiation produces less H_2O_2

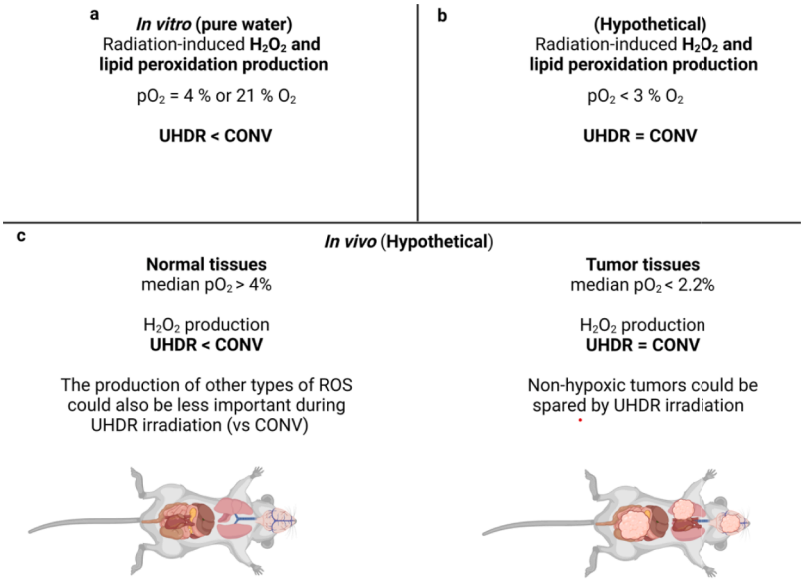

Fig. 1. Hypothetical model of ROS production by UHDR and CONV irradiation. **a)** Above 3.9 % O_2, UHDR irradiation induces a lower H_2O_2 generation than CONV irradiation in pure water or chemical based-models [87,102,104] (Sunnerberg et al., 2023; Kacem et al., 2022; Froidevaux et al., 2023). **b)** Below 4 % O_2, the potential difference between UHDR and CONV irradiation on H_2O_2 production is still unknown but the results in [84,87,104] (Sunnerberg et al., 2023; El Khatib et al., 2022; Froidevaux et al., 2023), suggest that there is no difference for UHDR compared to CONV irradiations in the production of H_2O_2 and lipid peroxidation below 3 % O_2. **c)** Based on the results performed *in vitro*, it is possible that a differential effect in H_2O_2 production and lipid peroxidation for UHDR compared to CONV irradiation occurs only in normal tissues, since the pO_2 is above 4% O_2 in most of them. On the other hand, since the pO_2 in tumor tissues is mostly below 2.2 % O_2, it is possible that there is no difference for UHDR compared to CONV irradiations in the production of H_2O_2 (and of other ROS), and hence no difference in tumor control. Furthermore, these results suggest that non-hypoxic tumors could be "spared" by UHDR irradiation and show the importance of testing this experimentally. Created with Biorender.com.

(and likely other ROS as well) than CONV irradiation, specifically in normal tissues, but not in tumors, due to their intrinsically different oxygenation levels (Fig. 1).

This is consistent with studies showing an impairment of the FLASH sparing effect via modification of the oxygenation status in normal tissue or via the use of antioxidant molecules [26,62]. Nonetheless, this would mean that well-oxygenated tumors could be spared by UHDR irradiation, and it would be very interesting to test whether the increase in pO_2 in the tumor, which could be induced by mild hyperthermia [107] or by hyperbaric oxygen therapy [108], would also protect tumors exposed to UHDR irradiation.

3.3. *Differences in the antioxidant pool between normal and tumor tissues and the need to investigate ROS production during UHDR and CONV irradiation in vivo*

The difference in ROS levels produced during UHDR versus CONV irradiation may support the theory of Spitz et al., who proposed that a differential antioxidant capability in cancer versus normal tissues would be the basis for explaining the FLASH effect [109]. More specifically, the smaller pool of labile iron (limiting Fenton-type reactions) and faster detoxification of radicals in normal tissues would result in a lower concentration of organic hydroperoxides compared to cancer tissues when the dose is delivered at the UHDR. This differential response would disappear at the CONV, because the antioxidant system of both types of tissue would efficiently annihilate the radicals generated during the irradiation pulse.

The model proposed by Labarbe et al. correlated IR-induced damage with the concentration of peroxyl radicals. More specifically, UHDR irradiation results in a high transient production of peroxyl radicals, leading to more local recombination between these radicals and, consequently, protection of the entire irradiated volume [110]. Hu et al. continued their investigations along this path, suggesting that the differential effect observed in normal and tumor tissues at UHDR irradiation is derived from the higher concentration of antioxidants present in neoplastic tissues. In normal tissues, the physiological antioxidant pool becomes saturated with IR-produced ROS and is unable to fully protect cells from the cytotoxic effects of these species. However, when ionizations are close in time, that is, at the UHDR, the recombination of radicals may participate in the overall decrease in ROS. This would not be the case in tumor tissues, where a higher concentration of antioxidants would be sufficient to tackle the ROS insult, regardless of the recombination mechanism, resulting in the same cytotoxic effects in CONV and UHDR irradiation [111]. Based on these *in silico* and *in vitro* results, the impact of the dose rate on the yield of radical species deserves further investigation, particularly for hydroxyl or superoxide radicals, owing to their high reactivity, but also for hydrogen peroxide. Indeed, most, if not all, studies so far that have been performed *in silico* or *in vitro,* do not fully recapitulate the complexity of *in vivo* models, and hence, are poorly representative of what really happens in irradiated tissues. Some techniques that seem relevant in the FLASH field are described in Section 4 with the aim of experimentally measuring *in vivo* the yield of ROS resulting from UHDR irradiation.

4. Methods to assess ROS production during irradiation

The oxygen concentration in irradiated tissues plays a prominent role in the generation of the FLASH effect, potentially affecting the yield of different ROS after irradiation. These reactive species can potentially have a tremendous effect on cell fate, impacting many cellular functions and triggering life-threatening processes such as lipid peroxidation. It is worth investigating whether an increase in the radiation dose rate affects the production of these species in *in vivo* models, including the degree of complexity that cannot be considered in *in silico* simulations and cell-free models. The following paragraph describes the experimental methodologies aimed at providing new insights into ROS production after UHDR irradiation. Although this objective is highly complex, investigations focusing on the production of primary radicals and their oxidative products are fundamental in obtaining a clearer and more complete view of the events occurring downstream of UHDR irradiation.

Although mass spectrometry (MS) has been extensively used to detect lipid peroxidation and protein oxidation (end products of ROS reactions) [112,113], investigations regarding the generation of primary radicals have not progressed in recent years. The following list of methodologies aims to stimulate investigations as a possible roadmap, proposing techniques that can circumvent the obstacles set by the intrinsic nature of ROS (short lifespan and low concentration). Currently, investigations regarding radical production rely mainly on *in silico* models, the reliability of which is frequently questioned owing to the (over)simplifications introduced to run the simulations [114]. In this context, the experimental assessment of primary ROS using the methodologies listed below could overcome this limitation, allowing direct measurement in a more physiological context.

4.1. *Bioluminescence*

Bioluminescence corresponds to the emission of light during luciferin oxidation by the enzyme luciferase. Peroxy-caged luciferin-1 (PCL-1) technology has been used for the *in vivo* detection of ROS [115]. Basically, in the absence of specific ROS, luciferin is "caged," preventing its oxidation and light emission. In the presence of ROS or reactive nitrogen species (RNS), such as H_2O_2, hypochlorite (HOCl), or peroxynitrite ($ONOO^-$), luciferin becomes accessible and can be oxidized by luciferase with the concomitant emission of light, which can be quantified by bioluminescence imaging [115,116]. This type of indirect measurement has been successfully used in murine tumor, peritoneal cavity, and testis models [115,117]. Bioluminescence was detected up to 1 h after injection of H_2O_2 into the peritoneal cavity in a concentration-dependent manner [115]. Furthermore, *in vitro* investigations showed that light emission reached its maximum level 10 min after the incubation of PCL-1 with H_2O_2, HOCl, or $ONOO^-$ [116]. Therefore, this technique allows the assessment of ROS/RNS production during or immediately after irradiation.

4.2. *Positron emission tomography tracers*

Positron emission tomography (PET) is a relatively noninvasive technique [118] that has several clinical and preclinical applications in oncology, neurology, and cardiology. This technology has recently been used to detect ROS in several preclinical models. Radiotracer ^{18}F-DHMT has attracted increasing interest in this context [119–121]. In the presence of superoxide, this compound is oxidized and binds to DNA, persisting for a prolonged period, whereas it is quickly cleared in the absence of superoxide. After 60 min of treatment with doxorubicin, the radioactivity detected in the hearts of mice corresponded to the oxidized form of ^{18}F-DHMT [120]. Nonetheless, the time for which the compound remains oxidized once superoxide production through IR is complete is unknown. Another PET tracer, galuminox [122], is weakly fluorescent, but is oxidized in the presence of superoxide or H_2O_2 and becomes highly fluorescent. Hence, this compound could be used in transparent animals such as zebrafish, a model often used in FLASH studies. Recently, a study showed a FLASH effect in another transparent model, the *C. elegans* worm; therefore, this tracer could also be used in this model [27]. There was a threefold higher retention of this compound in the lungs of mice treated with lipopolysaccharide (LPS), a known inducer of ROS production in the lungs. Nonetheless, the time required for the compound to revert to its unoxidized form and be cleared from the organ of interest remains unknown. In conclusion, certain PET tracers can be used to assess superoxide and/or hydrogen peroxide production shortly after irradiation. However, it should be assessed whether their oxidized forms are stable and for how long.

4.3. Upconverting nanoparticle-based near-infrared nanoprobes

Fluorescence-based techniques can also be implemented to detect ROS production in biological systems, with probes absorbed in the near-infrared (NIR) region being the most promising because of the low interference from the system under investigation. Upconverting nanoparticles (UCNPs) are frequently used for this purpose and offer high tissue penetration, low toxicity, and high physical/chemical stability when injected *in vivo* [123]. Most of the time, UCNPs are coupled with appropriate energy acceptors that absorb the energy emitted from the nanoparticles through linear resonance energy transfer (LRET) and re-emit it at higher frequencies. ROS detection occurs when the radical reacts with the acceptor, which enables (or prevents) LRET and the corresponding detection of signals from the energy acceptor (or from the UCNPs themselves). The flexibility of this approach represents its main strength, enabling the modification of the absorption spectra of the energy donor using different dopants or energy acceptors that selectively react with any ROS species. According to the energy acceptor and dopants used, the emission of fluorescence (following the reaction with ROS) can be in either the NIR wavelength (above 750 nm, permitting its detection in living animals) or in the visible light range. For the latter, the signal can be directly detected in transparent animals such as zebrafish, whereas tissue sections can be used for nontransparent models.

In this context, Li et al. developed an *in vivo* probe to detect hydroxyl radicals in murine liver sections by coupling sandwich-structured UCNPs with an azo dye (which quenches the fluorescence of the UCNPs); this system provides a linear response between upconverted luminescence (UCL) and $OH^{\bullet}$ radical concentration in the 2–195 fM range [124]. The azo dyes of these probes decompose in the presence of $OH^{\bullet}$ radicals, suggesting that UCNPs can emit fluorescence for a prolonged period following azo dye decomposition. Indeed, the longer the probe was incubated in the liver, the higher the fluorescence intensity.

Following the same principle as ROS detection, changing the energy acceptor enabled several groups to detect specific types of ROS or nonspecific ROS in living organisms. Hao et al. measured H_2O_2 levels *in vitro* and *in vivo* in mice [125]. By changing the dopant and shifting from Yb^{3+} to Nd^{3+}, Wang et al. tuned the spectral properties of the energy donor; they reduced the absorption wavelength of the nanoparticles to 808 nm to lower overheating due to water absorption and specifically studied H_2O_2 production in cells and living mice [126]. Finally, an NIR fluorescent probe was developed to accurately detect the superoxide radical levels in ferroptosis-mediated epilepsy in mouse tissue sections [127].

In summary, LRET-based UNCPs have great potential for ROS detection in small animals, enabling high physical/chemical stability while providing high tissue penetration and almost no toxicity upon injection. Furthermore, the flexibility provided by the energy donor/acceptor couple allows the measurement of specific ROS concentrations and reduces the interference that could arise from other reactive species in living animals (transparent or not) and in animal tissue sections.

4.4. Aromatic hydroxylation

ROS can also be detected indirectly by targeting the adducts formed through reactions with suitable substrates rather than the radical itself. Once formed, the hydroxylated products can be separated and directly measured using liquid chromatography-mass spectrometry (LC-MS). This approach can be used to detect highly reactive radicals such as hydroxyl radicals by causing them to react with aromatic compounds. Salicylate and phenylalanine have already been used for this type of application because hydroxylated products are not endogenously present within cells as metabolites [128,129]. However, the application of these substrates for ROS detection *in vivo* has recently been questioned because of the great impact of the intracellular chemical environment on the hydroxylation process [130]. An interesting alternative is benzoic acid derivatives, a family of probes that become fluorescent upon reaction with highly reactive ROS [131].

4.5. Genetically encoded redox biosensors

Genetically encoded redox biosensors (GERB) are genetically encoded fluorescent proteins that exist in oxidized or reduced forms with different fluorescence profiles. Hence, these biosensors are ratiometric, meaning that the global expression of the proteins is not important, but rather the fluorescence ratio between the oxidized and reduced forms. These probes are genetically encoded, and hence can be expressed in specific cell types or in specific cell compartments, enabling the detection of the signal directly from transparent models (such as zebrafish); however, they have also been successfully used in nontransparent models (such as mice). According to the type of GERB, the protein can be sensitive to redox status (glutathione/glutathione disulphide (GSH/GSSG) ratio), nicotinamide adenine dinucleotide hydrogen/nicotinamide adenine dinucleotide+ (NADH/NAD+) ratio, or presence of H_2O_2 [132]. In this study, we focused on the H_2O_2-sensitive biosensors.

There are two families of H_2O_2-sensitive GERBs: the HyPer family and the redox-sensitive green fluorescence protein 2 (roGFP2) family. Seven versions of HyPer have been developed: HyPer, Hyper-2, Hyper-3, Hyper-7, HyPer-H34Y-A406V, TriPer, and HyPerRed. For most of them, the kinetics of oxidation and reduction are very fast and can hence be used for real-time monitoring of H_2O_2 production. Among the HyPer proteins, only HyPer-7 is insensitive to pH, which seems very interesting in the UHDR field because the intracellular and extracellular pH of normal and tumor tissues are slightly different [133,134]. In chloroplasts, the intensity ratio between oxidized and reduced probe fluorescence was reduced by 10 % after 10 min of H_2O_2 stimulation and by 25 % after 20 min [135]. Considering the rapid decrease in the signal, it could find application as a live probe, with the fluorescent output being measured during irradiation.

At least two types of roGFP2 can be used to assess H_2O_2 level *in vivo*: roGFP2-Orp1 and roGFP2-Tsa2 (and its variant ΔCR) [136–138]. However, roGFP2-Orp1 is sensitive to other intracellular oxidants [139,140]. On the other hand, roGFP2-Tsa2ΔCR is much less impacted by other oxidants, making it a more appropriate probe for H_2O_2 detection [136]. Furthermore, after stimulation of yeast by H_2O_2, roGFP2-Tsa2ΔCR showed a prolonged augmentation of its oxidized/reduced ratio, (lasting for about 20 to 100 min, according to H_2O_2 concentration), compared with roGFP2-Orp1 or HyPer proteins (several seconds/minutes) [136]. Hence, roGFP2-Tsa2ΔCR seems to be the most interesting GERB for assessing H_2O_2 production during irradiation, because once oxidized, the reduction rate is strongly slower than for other GERBs. However, this reduction rate was assessed only in yeast, and it would be interesting to assess this rate using other models.

4.6. Mass spectrometry

MS is another technique that allows the rapid and highly accurate detection of several ROS. Although techniques based on fluorescent probes may produce adducts, increasing the noise of the measurement, MS enables a more accurate measurement of specific adducts through a change in the mass-to-charge ratio (m/z). This approach has been extensively used to detect many radical species both *in vivo* and *in vitro* (already reviewed in [100]). For instance, Portier et al. reported altered dynamics of oxylipins in response to radiation, with a dependence on the dose rate and oxygen status. More specifically, irradiation of normal cells (but not cancer cells) at the CONV induces a more prominent increase in oxylipins than UHDR irradiation [141].

5. Implications of irradiation-induced ROS on cell fate

5.1. Mitochondria

Irradiation causes an increase in mitochondrial ROS (mtROS), creating a pro-oxidative environment and starting a vicious cycle eventually leading to impairment of the organelle functions (a process called "ROS-induced ROS release") [142,143]. As hypothesized by Vozenin and Limoli, CONV and UHDR irradiation may have different effects on mitochondrial metabolism, mtROS production, and the electron transport chain [10]. Similarly, Guo et al. showed that irradiation of normal cells (IMR90 fibroblasts) at a UHDR preserved mitochondrial structure, copy number, and the overall mitochondrial network, with a smaller impact on mitochondrial functions when compared to CONV irradiation (ATP production after UHDR irradiation was approximately 13 % higher than CONV irradiation). Mitochondrial dynamics followed the same trend, with lower colocalization of Drp-1/p53 in the UHDR-irradiated group. Furthermore, the mean mitochondrial length was strongly diminished by CONV irradiation but was unaffected by UHDR irradiation in normal cells. However, in A549 lung cancer cells, the mitochondrial network structure was equally affected by both irradiation regimens [50]. Nonetheless, the authors did not specifically assess mtROS production according to the dose rate. Given the impact of the oxidative environment on mitochondrial health, we think that it is worth focusing on this organelle because UHDR irradiation appears to limit the production of H_2O_2 and possibly other radicals in normal tissues. Investigating the oxidative environment within mitochondria could be performed through probes that specifically target this organelle (e.g., MitoSOX and MitoTEMPO, respectively, to detect and protect the organelle from the deleterious effect of superoxide radicals, respectively), or by introducing ROS-detecting molecules (such as dihydroethidium), or spin traps (DEPMPO) in the mitochondrial matrix by coupling these molecules with triphenylphosphonium, a mitochondriotropic carrier that allows increasing the concentration of the cargo within the organelle by two orders of magnitude [144]. These methods may offer valuable insights into the oxidative state within the mitochondrial matrix, which is particularly relevant for free-radical-induced lipid peroxidation of cardiolipin, a phospholipid located exclusively in the inner mitochondrial membrane.

Interestingly, several studies have linked H_2O_2 to the pseudo-peroxidase activity of cytochrome *c* [145,146], whose complex can initiate the radical process via hydrogen abstraction from one of the cardiolipin side chains. In this context, the reduced production of H_2O_2 in normal tissues after UHDR irradiation (Fig. 1) could result in less oxidation of lipids in the inner mitochondrial membrane, protecting the organelles from the deleterious effects of IR (Fig. 2).

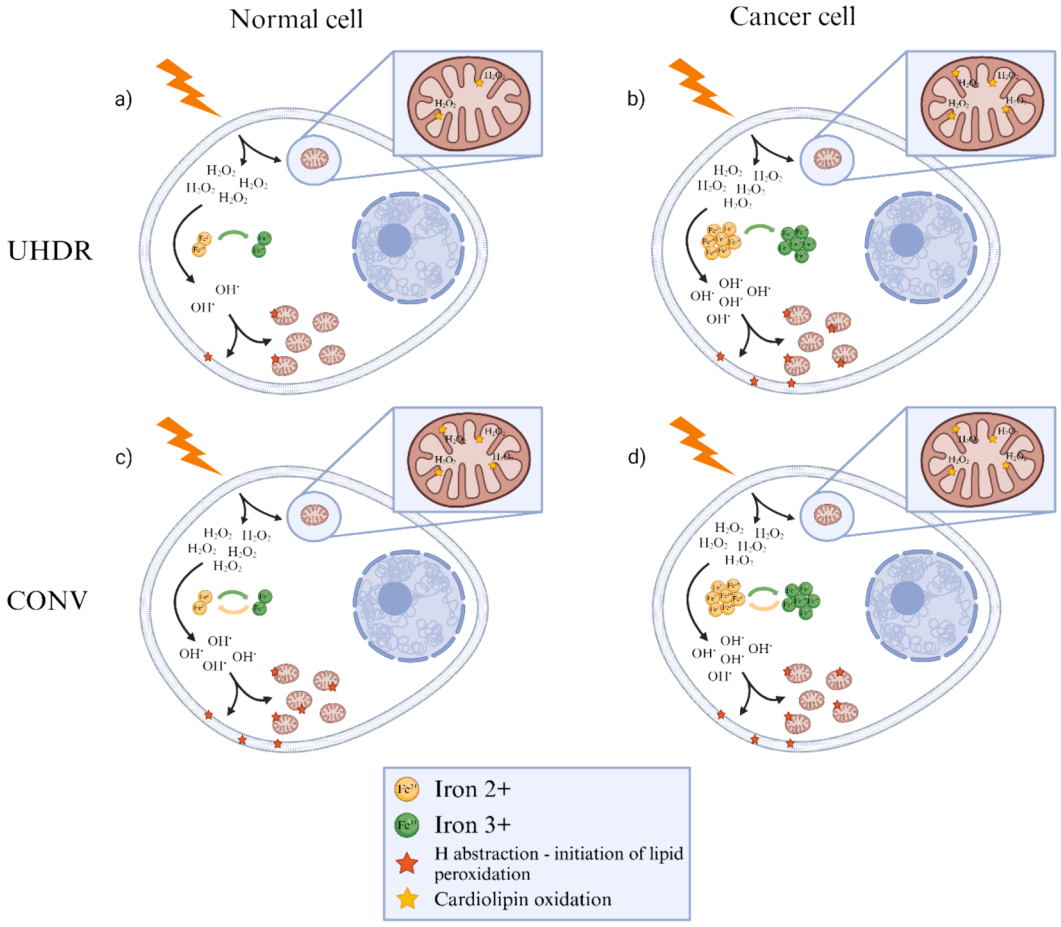

Fig. 2. Hypothetical model of ROS-induced damage by ultra-high dose rate (UHDR) vs conventional dose rate (CONV). In the hypothetical mechanism we propose, the differential cytotoxicity of UHDR compared to CONV could depend on different levels of radiolytic H_2O_2 (and, maybe, of other ROS) production. Briefly, at UHDR, the short irradiation time generates a peak in H_2O_2, that saturates the iron pool of normal cells (a), but not of the cancer ones (b), preventing its regeneration and its availability for other Fenton reactions. In addition, the lower radiolytic yield of H_2O_2 in normal cells would result in a lower oxidation of cardiolipin by the pseudo-peroxidase H_2O_2-cyt c complex, protecting mitochondria from the deleterious effect of ionizing radiation. On the other hand, the longer irradiation time at CONV dose rate would allow the regeneration of Fe^{2+} and its implication in further Fenton reactions, resulting in higher amount of $OH^{\cdot}$ radicals (c and d). Hence, the lower H_2O_2 yield in normal cells at UHDR irradiation, and the saturation of iron pool would limit the extent of lipid and cardiolipin oxidation, whereas no difference would be observed in UHDR irradiated tumor cells (vs CONV irradiated). Created with Biorender.com.

To our knowledge, only one study investigating the mitochondrial response after UHDR irradiation has been published [50]. Further investigations could provide interesting insights into the mechanisms underlying the effects of FLASH.

5.2. The potential role of ferroptosis

An altered oxidative environment could also impact ferroptosis, a non-apoptotic cell death triggered by weakening of the antioxidant potential and consequent accumulation of lipid peroxides (LOOH) [147,148]. These molecules are most frequently generated as a consequence of the abstraction of an allylic hydrogen in polyunsaturated fatty acid (PUFA) by highly reactive radicals such as $OH^{\bullet}$, $HO_2^{\bullet}$, or other $RO^{\bullet}$. Furthermore, ferroptosis is involved in irradiation-induced damage to normal tissues, such as the intestine, heart, lung, and skin [149].

A direct correlation between the IR dose and lipid peroxidation has been known for decades [150,151], and irradiation-induced ROS have been proposed as initiators of this process [152]. The impact of radiation dose rate on the initiation of the oxidative cascade was investigated at the beginning of the 1990s. Although not measured in the UHDR regime, lipid peroxidation has been shown to be positively correlated with the concentration of Fe^{2+} ions and, more interestingly, negatively correlated with the dose rate, with lower lipid peroxidation as the dose rate increased [153–156]. In these studies, the inverse correlation between the induction of lipid peroxidation and the dose rate was termed the "inverse dose-rate effect" [157].

Regarding the UHDR regime, Froidevaux et al. were the first to investigate the impact of radiation dose rate on lipid peroxidation, showing a dose-dependent production of peroxidation end products (namely, LOOH and malondialdehyde (MDA)) at CONV irradiation, while no induction of lipid peroxidation was observed at UHDR irradiation (> 540 Gy/s) in a chemical-based model. Oxygen was also shown to affect this process when irradiation was performed at CONV irradiation, with a peroxidation yield that was halved at 4 % O_2 compared with that at 21 % O_2 [104].

This observation was further confirmed by the only *in vivo* study assessing the link between peroxidation yield and dose rate, with UHDR irradiation inducing less lipid peroxidation than CONV irradiation after abdominal irradiation in mice, 24 h after irradiation [158].

This oxidative process has attracted increasing interest in the FLASH community, especially when coupled with the free iron pool within cells and ferroptosis [10,147,148,153,159]. Excessive iron levels are associated with tumorigenesis and are hallmarks of cancer [160–163]. In the context of lipid peroxidation, iron is very important because it catalyzes the formation of highly reactive hydroxyl radicals through the Fenton and Haber-Weiss reactions. The resulting hydroxyl radicals help cancer cells acquire new cancer hallmarks [164,165] and initiate lipid peroxidation by abstracting the allylic hydrogen of unsaturated lipid chains. Vilaplana-Lopera [159] recently postulated an interesting theory to explain the differential responses to radiation at the UHDR in tumors versus normal tissues, linking the altered iron pool, lipid peroxidation, and the corresponding induction of ferroptosis. In this model, the combination of oxygen depletion induced by the UHDR and physiological iron content protects normal cells from lipid peroxidation and, ultimately, induces less ferroptosis compared to cancer cells, where the even lower oxygen concentration is counterbalanced by the deregulated free iron content. This also explains the *iso*-efficacy observed for UHDR versus CONV irradiation in tumor tissues.

However, because radiation has been shown to marginally deplete O_2 in living tissues (Section 2), ROD is unlikely to be the initial step in the induction of the FLASH effect. Therefore, we propose a slightly different and ROD-independent mechanism, based on a differential production of hydroxyl radicals via Fenton reaction, and introducing the concept of "saturation" of the Fe^{2+} catalyst (Fig. 2). The extremely short time required to irradiate normal tissues at the UHDR does not allow the physiological pool of Fe^{3+} to be regenerated, whereas radiation-induced H_2O_2 species are still present, limiting the production of reactive $OH^{\bullet}$ and, consequently, the extent of lipid peroxidation. At CONV irradiation, the longer time required to perform irradiation allowed the reduction of Fe^{3+} to Fe^{2+}, fueling other Fenton reactions and increasing the amount of $OH^{\bullet}$ radicals. In contrast, a larger labile iron pool within tumor tissues produces more $OH^{\bullet}$ radicals, independent of the dose rate. To test this hypothesis, iron-sequestering molecules, such as transferrin or caeruloplasmin, could be used to stabilize the iron redox state (and prevent its catalytic action in Fenton reactions). Additionally, inhibitors of ferroptosis, such as liproxstatin-1 or ferrostatin-1, would allow us to determine whether this process is directly involved in the differential effect observed in UHDR versus CONV irradiation.

5.3. ROS/senescence/inflammation positive feedback loop

Senescent cells are in irreversible cell cycle arrest but are still metabolically active. Radiotherapy-induced senescence is strongly associated with radiation-induced normal tissue injuries [166–168]. Nevertheless, to our knowledge, only a few studies have investigated the effect of UHDR irradiation on senescence induction. *In vitro*, it was shown that UHDR proton irradiation induced a less important proportion of senescence-associated β galactosidase positive cells than CONV irradiation, in IMR90 fibroblasts [54]. *In vivo*, FLASH irradiation induced a less important senescence-associated β galactosidase activity as well as expression of senescence-associated markers in irradiated mouse lung, compared with CONV irradiation [169].

It is well known that the overproduction of ROS (induced by radiotherapy or other stimuli) can induce cell senescence via DNA damage-dependent and −independent processes [167,170–172]. Dysfunctional mitochondria producing high levels of ROS and senescence-associated secretory phenotype (SASP) are other hallmarks of senescent cells [173].

Senescent features are not locally confined, but may spread through the SASP, whose composition is dynamic, stress-dependent, and heterogeneous. The SASP comprises cytokines, chemokines, and growth factors, which are released within the extracellular environment, promoting chronic inflammation and tissue fibrosis in neighboring healthy tissues [167,168,170].

Excessive oxidative stress can lead to an auto-sustained loop between senescence, ROS production, and chronic inflammation [168,170,174]. Hence, it would be worth investigating the impact of UHDR irradiation on the overall picture, because this kind of irradiation induces a lower production of ROS than CONV irradiation, and hence, less senescence [54,169]. The protective effect of FLASH-RT could, at least in part, be derived from the reduced induction of the senescence phenotype, which could be tested by administering senolytic drugs upon CONV and UHDR irradiation [168].

6. Concluding remarks

FLASH RT may have a significant impact on the RT field, allowing the expansion of the therapeutic window owing to its limited toxicity to normal tissues. However, despite great interest in this treatment modality, the underlying mechanism(s) is not completely understood, and a mechanistic description is still missing.

Although initial theories postulated that the sparing of normal tissues was ascribable to transient hypoxia and/or a reduced amount of DNA damage, further investigations undermined the basis of these theories. Recent studies have suggested that the radiation dose rate can impact H_2O_2 (and other ROS) production. However, this dependence is valid only for cells at physiological oxygen concentrations, whereas no differences have been predicted for tissues under hypoxic conditions (such as tumors). Hence, we speculate that there could be lower H_2O_2 generation following UHDR irradiation, specifically in normal tissue but not in tumor tissue, due to the difference in the basal oxygenation levels of these tissues (Fig. 1). Furthermore, the lower iron-labile pool in normal cells, combined with the short timeframe of UHDR irradiation,

allow for a specific decrease in lipid peroxidation in normal cells (Fig. 2). This difference could have crucial implications, giving rise to a smaller amount of highly reactive hydroxyl radicals (produced through the Fenton reaction) and/or reducing the extent of cardiolipin oxidation in healthy tissues, thus limiting mitochondrial damage. This could also give rise to the less important induction of senescence in normal tissues.

Although technically challenging, the differences in cytosolic and mtROS production between the two irradiation regimes should be confirmed *in vivo* in both normal and tumor tissues. The methodologies proposed in this review can potentially answer this question, providing new experimental insights into what occurs immediately after irradiation.

CRediT authorship contribution statement

Andrea Scarmelotto: Conceptualization, Methodology, Writing – original draft, Writing – review & editing. **Victor Delprat:** Conceptualization, Methodology, Writing – original draft, Writing – review & editing. **Carine Michiels:** Project administration, Supervision, Writing – review & editing. **Stéphane Lucas:** Funding acquisition, Project administration, Supervision, Writing – review & editing. **Anne-Catherine Heuskin:** Methodology, Project administration, Supervision, Writing – review & editing.

Declaration of competing interest

The authors declare that they have no known competing financial interests or personal relationships that could have appeared to influence the work reported in this paper.

Acknowledgements

The EPT project (Emerging Proton Therapy) is financed by the Public Service of Wallonia via the MecaTech competitiveness cluster (convention 8341). In addition, the authors thank Dr. Penninckx Sebastien for the useful discussions and the support provided during the design of the manuscript.

References

[1] Chargari C, et al. Optimize and refine therapeutic index in radiation therapy: overview of a century. Cancer Treat Rev 2016;45:58–67. https://doi.org/10.1016/j.ctrv.2016.03.001.
[2] Hong TS, Ritter MA, Tomé WA, Harari PM. Intensity-modulated radiation therapy: emerging cancer treatment technology. Br J Cancer 2005;92(10):1819–24. https://doi.org/10.1038/sj.bjc.6602577.
[3] Moghaddasi L, Reid P, Bezak E, Marcu LG. Radiobiological and treatment-related aspects of spatially fractionated radiotherapy. Int J Mol Sci. 2022;23(6):6. https://doi.org/10.3390/ijms23063366.
[4] Reda M, Bagley AF, Zaidan HY, Yantasee W. Augmenting the therapeutic window of radiotherapy: a perspective on molecularly targeted therapies and nanomaterials. Radiother Oncol 2020;150:225–35. https://doi.org/10.1016/j.radonc.2020.06.041.
[5] Epp ER, Weiss H, Djordjevic B, Santomasso A. The radiosensitivity of cultured mammalian cells exposed to single high intensity pulses of electrons in various concentrations of oxygen. Radiat Res 1972;52(2):324–32. https://doi.org/10.2307/3573572.
[6] Field SB, Bewley DK. Effects of dose-rate on the radiation response of rat skin. Int J Radiat Biol Relat Stud Phys Chem Med 1974;26(3):259–67. https://doi.org/10.1080/09553007414551221.
[7] Inada T, Nishio H, Amino S, Abe K, Saito K. High dose-rate dependence of early skin reaction in mouse. Int J Radiat Biol Relat Stud Phys Chem Med 1980;38(2):139–45. https://doi.org/10.1080/09553008014551031.
[8] Town CD. Effect of high dose rates on survival of mammalian cells. Nature 1967;215(5103):5103. https://doi.org/10.1038/215847a0.
[9] Favaudon V, et al. Ultrahigh dose-rate FLASH irradiation increases the differential response between normal and tumor tissue in mice. Sci Transl Med 2014;6(245):245ra93. https://doi.org/10.1126/scitranslmed.3008973.
[10] Limoli CL, Vozenin M-C. Reinventing radiobiology in the light of FLASH radiotherapy. Annu Rev Cancer Biol 2023;7(1):1–21. https://doi.org/10.1146/annurev-cancerbio-061421-022217.
[11] Kacem H, Almeida A, Cherbuin N, Vozenin M-C. Understanding the FLASH effect to unravel the potential of ultra-high dose rate irradiation. Int J Radiat Biol 2022;98(3):506–16. https://doi.org/10.1080/09553002.2021.2004328.
[12] Montay-Gruel P, et al. Irradiation in a flash: Unique sparing of memory in mice after whole brain irradiation with dose rates above 100Gy/s. Radiother Oncol 2017;124(3):365–9. https://doi.org/10.1016/j.radonc.2017.05.003.
[13] Liu K, et al. Redefining FLASH RT: the impact of mean dose rate and dose per pulse in the gastrointestinal tract. bioRxiv 2024. https://doi.org/10.1101/2024.04.19.590158.
[14] Romano F, Bailat C, Jorge PG, Lerch MLF, Darafsheh A. Ultra-high dose rate dosimetry: challenges and opportunities for FLASH radiation therapy. Med Phys 2022;49(7):4912–32. https://doi.org/10.1002/mp.15649.
[15] Vozenin M-C, Montay-Gruel P, Limoli C, Germond J-F. All irradiations that are ultra-high dose rate may not be FLASH: the critical importance of beam parameter characterization and in vivo validation of the FLASH effect. Radiat Res 2020;194(6):571–2. https://doi.org/10.1667/RADE-20-00141.1.
[16] Di Martino F, et al. Architecture, flexibility and performance of a special electron linac dedicated to Flash radiotherapy research: electronFlash with a triode gun of the centro pisano flash radiotherapy (CPFR). Front Phys 2023;11. https://doi.org/10.3389/fphy.2023.1268310.
[17] Vozenin M-C, et al. The advantage of FLASH radiotherapy confirmed in mini-pig and cat-cancer patients. Clin Cancer Res 2019;25(1):35–42. https://doi.org/10.1158/1078-0432.CCR-17-3375.
[18] Rohrer Bley C, et al. Dose- and volume-limiting late toxicity of FLASH Radiotherapy in cats with squamous cell carcinoma of the nasal planum and in mini pigs. Clin Cancer Res 2022;28,(17):3814–23. https://doi.org/10.1158/1078-0432.CCR-22-0262.
[19] Konradsson E, et al. Establishment and initial experience of clinical FLASH radiotherapy in canine cancer patients. Front Oncol 2021;11:658004. https://doi.org/10.3389/fonc.2021.658004.
[20] Børresen B, et al. Evaluation of single-fraction high dose FLASH radiotherapy in a cohort of canine oral cancer patients. Accessed: Oct. 15, 2023. [Online]. Available: Front Oncol 2023;13.
[21] Bourhis J, et al. Treatment of a first patient with FLASH-radiotherapy. Radiother Oncol 2019;139:18–22. https://doi.org/10.1016/j.radonc.2019.06.019.
[22] Gaide O, et al. Comparison of ultra-high versus conventional dose rate radiotherapy in a patient with cutaneous lymphoma. Radiother Oncol 2022;174:87–91. https://doi.org/10.1016/j.radonc.2021.12.045.
[23] Saade G, et al. Ultrahigh-dose-rate proton irradiation elicits reduced toxicity in zebrafish embryos. Adv Radiat Oncol 2023;8(2):101124. https://doi.org/10.1016/j.adro.2022.101124.
[24] Beyreuther E, et al. Feasibility of proton FLASH effect tested by zebrafish embryo irradiation. Radiother Oncol 2019;139:46–50. https://doi.org/10.1016/j.radonc.2019.06.024.
[25] Karsch L, et al. Beam pulse structure and dose rate as determinants for the flash effect observed in zebrafish embryo. Radiother Oncol J Eur Soc Ther Radiol Oncol 2022;173:49–54. https://doi.org/10.1016/j.radonc.2022.05.025.
[26] Montay-Gruel P, et al. Long-term neurocognitive benefits of FLASH radiotherapy driven by reduced reactive oxygen species. Proc Natl Acad Sci 2019;116(22):10943–51. https://doi.org/10.1073/pnas.1901777116.
[27] Schoenauen L, Stubbe F-X, Van Gestel D, Penninckx S, Heuskin A-C. C. elegans: a potent model for high-throughput screening experiments investigating the FLASH effect. Clin Transl Radiat Oncol 2023;45:100712. https://doi.org/10.1016/j.ctro.2023.100712.
[28] Tinganelli W, et al. FLASH with carbon ions: tumor control, normal tissue sparing, and distal metastasis in a mouse osteosarcoma model. Radiother Oncol 2022;175:185–90. https://doi.org/10.1016/j.radonc.2022.05.003.
[29] Ghannam Y, et al. First evidence of *in vivo* effect of FLASH radiotherapy with helium ions in zebrafish embryos. Radiother Oncol 2023;187:109820. https://doi.org/10.1016/j.radonc.2023.109820.
[30] Montay-Gruel P, et al. Hypofractionated FLASH-RT as an effective treatment against glioblastoma that reduces neurocognitive side effects in mice. Clin Cancer Res 2021;27(3):3. https://doi.org/10.1158/1078-0432.CCR-20-0894.
[31] Montay-Gruel P, et al. Ultra-high-dose-rate FLASH irradiation limits reactive gliosis in the brain. Radiat Res 2020;194(6):636–45. https://doi.org/10.1667/RADE-20-00067.1.
[32] Montay-Gruel P, et al. X-rays can trigger the FLASH effect: Ultra-high dose-rate synchrotron light source prevents normal brain injury after whole brain irradiation in mice. Radiother Oncol J Eur Soc Ther Radiol Oncol 2018;129(3):3. https://doi.org/10.1016/j.radonc.2018.08.016.
[33] Simmons DA, et al. Reduced cognitive deficits after FLASH irradiation of whole mouse brain are associated with less hippocampal dendritic spine loss and neuroinflammation. Radiother Oncol J Eur Soc Ther Radiol Oncol 2018;139:4–10. https://doi.org/10.1016/j.radonc.2019.06.006.
[34] Alaghband Y, et al. Neuroprotection of radiosensitive juvenile mice by ultra-high dose rate FLASH irradiation. Cancers 2020;12(6):6. https://doi.org/10.3390/cancers12061671.
[35] Allen BD, et al. Maintenance of tight junction integrity in the absence of vascular dilation in the brain of mice exposed to ultra-high-dose-rate FLASH irradiation. Radiat Res 2020;194(6):6. https://doi.org/10.1667/RADE-20-00060.1.
[36] Gao F, et al. First demonstration of the FLASH effect with ultrahigh dose rate high-energy X-rays. Radiother Oncol 2022;166:44–50. https://doi.org/10.1016/j.radonc.2021.11.004.
[37] Evans T, Cooley J, Wagner M, Yu T, Zwart T. Demonstration of the FLASH effect within the spread-out bragg peak after abdominal irradiation of mice. Int. J. Part. Ther 2022;8(4):4. https://doi.org/10.14338/IJPT-20-00095.
[38] Ruan J-L, et al. Irradiation at ultra-high (FLASH) dose rates reduces acute normal tissue toxicity in the mouse gastrointestinal system. Int J Radiat Oncol 2021;111(5):5. https://doi.org/10.1016/j.ijrobp.2021.08.004.

[39] Levy K, et al. Abdominal FLASH irradiation reduces radiation-induced gastrointestinal toxicity for the treatment of ovarian cancer in mice. Sci Rep 2020; 10(1):1. https://doi.org/10.1038/s41598-020-78017-7.
[40] Kim MM, et al. Comparison of FLASH proton entrance and the spread-out bragg peak dose regions in the sparing of mouse intestinal crypts and in a pancreatic tumor model. Cancers 2021;13(16):16. https://doi.org/10.3390/cancers13164244.
[41] Venkatesulu BP, et al. Ultra high dose rate (35 Gy/sec) radiation does not spare the normal tissue in cardiac and splenic models of lymphopenia and gastrointestinal syndrome. Sci. Rep 2019;9(1):1. https://doi.org/10.1038/s41598-019-53562-y.
[42] Diffenderfer ES, et al. Design, implementation, and in vivo validation of a novel proton FLASH radiation therapy system. Int J Radiat Oncol Biol Phys 2020;106 (2):2. https://doi.org/10.1016/j.ijrobp.2019.10.049.
[43] Soto LA, et al. FLASH irradiation results in reduced severe skin toxicity compared to conventional-dose-rate irradiation. Radiat Res 2020;1946:6. https://doi.org/10.1667/RADE-20-00090.
[44] Vozenin M-C, Hendry JH, Limoli CL. Biological benefits of ultra-high dose rate FLASH radiotherapy: sleeping beauty awoken. Clin Oncol 2019;31(7):7. https://doi.org/10.1016/j.clon.2019.04.001.
[45] Pawelke J, et al. Electron dose rate and oxygen depletion protect zebrafish embryos from radiation damage. Radiother Oncol 2021;158:7–12. https://doi.org/10.1016/j.radonc.2021.02.003.
[46] Beyreuther E, et al. Feasibility of proton FLASH effect tested by zebrafish embryo irradiation. Radiother Oncol J Eur Soc Ther Radiol Oncol 2019;139:46–50. https://doi.org/10.1016/j.radonc.2019.06.024.
[47] Saade G, et al. Ultrahigh-dose-rate proton irradiation elicits reduced toxicity in zebrafish embryos. Adv Radiat Oncol 2023;8(2):101124. https://doi.org/10.1016/j.adro.2022.101124.
[48] Adrian G, Konradsson E, Lempart M, Bäck S, Ceberg C, Petersson K. The FLASH effect depends on oxygen concentration. Br J Radiol Feb. 2020;93(1106): 20190702. https://doi.org/10.1259/bjr.20190702.
[49] Adrian G, et al. Cancer cells can exhibit a sparing FLASH Effect at low doses under normoxic in vitro-conditions. Front Oncol 2021;11. https://doi.org/10.3389/fonc.2021.686142.
[50] Guo Z, Buonanno M, Harken A, Zhou G, Hei TK. Mitochondrial damage response and fate of normal cells exposed to FLASH irradiation with protons. Radiat Res 2022;197(6):569–82. https://doi.org/10.1667/RADE-21-00181.1.
[51] Tessonnier T, et al. FLASH dose rate helium ion beams: first in vitro investigations. Int J Radiat Oncol Biol Phys 2021;111(4):4. https://doi.org/10.1016/j.ijrobp.2021.07.1703.
[52] Fouillade C, et al. FLASH irradiation spares lung progenitor cells and limits the incidence of radio-induced senescence. Clin Cancer Res 2020;26(6):1497–506. https://doi.org/10.1158/1078-0432.CCR-19-1440.
[53] Khan S, et al. Multicellular spheroids as in vitro models of oxygen depletion during FLASH irradiation. Int J Radiat Oncol Biol Phys 2021;110(3):3. https://doi.org/10.1016/j.ijrobp.2021.01.050.
[54] Buonanno M, Grilj V, Brenner DJ. Biological effects in normal cells exposed to FLASH dose rate protons. Radiother Oncol 2019;139:51–5. https://doi.org/10.1016/j.radonc.2019.02.009.
[55] Berry RJ, Stedeford JBH. Reproductive survival of mammalian cells after irradiation at ultra-high dose-rates: further observations and their importance for radiotherapy. Br J Radiol 1972;45(531):531. https://doi.org/10.1259/0007-1285-45-531-171.
[56] Nias AHW, Swallow AJ, Keene JP, Hodgson BW. Effects of pulses of radiation on the survival of mammalian cells. Br J Radiol 1969;42(499):499. https://doi.org/10.1259/0007-1285-42-499-553-b.
[57] Nias AHW, Swallow AJ, Keene JP, Hodgson BW. Survival of HeLa cells from 10 nanosecond pulses of electrons. Int J Radiat Biol Relat Stud Phys Chem Med 1970; 17(6):6. https://doi.org/10.1080/09553007014550751.
[58] Cygler J, Klassen NV, Ross CK, Bichay TJ, Raaphorst GP. The survival of aerobic and anoxic human glioma and melanoma cells after irradiation at ultrahigh and clinical dose rates. Radiat Res 1994;140(1):1. https://doi.org/10.2307/3578571.
[59] Zackrisson BU, Nyström UH, Ostbergh P. Biological response in vitro to pulsed high dose rate electrons from a clinical accelerator. Acta Oncol 1991;30(6):6. https://doi.org/10.3109/02841869109092451.
[60] Michaels HB, Epp ER, Ling CC, Peterson EC. Oxygen sensitization of CHO cells at ultrahigh dose rates: prelude to oxygen diffusion studies. Radiat Res 1978;76(3): 3. https://doi.org/10.2307/3574800.
[61] Berry RJ, Hall EJ, Forster DW, Storr TH, Goodman MJ. Survival of mammalian cells exposed to X rays at ultra-high dose-rates. Br J Radiol 1969;42(494):494. https://doi.org/10.1259/0007-1285-42-494-102.
[62] Zhang Q, et al. Proton FLASH effects on mouse skin at different oxygen tensions. Phys Med Biol Feb. 2023;68(5):055010. https://doi.org/10.1088/1361-6560/acb888.
[63] Iturri L, et al. Oxygen supplementation in anesthesia can block FLASH effect and anti-tumor immunity in conventional proton therapy. Commun Med 2023;3(1): 1–13. https://doi.org/10.1038/s43856-023-00411-9.
[64] "Anesthetic oxygen use and sex are critical factors in the FLASH sparing effect," Adv Radiat Oncol 2024;9(6):101492. 10.1016/j.adro.2024.101492.
[65] Hendry JH, Moore JV, Hodgson BW, Keene JP. The constant low oxygen concentration in all the target cells for mouse tail radionecrosis. Radiat Res 1982; 92(1):172. https://doi.org/10.2307/3575852.
[66] Leavitt RJ, et al. Acute hypoxia does not alter tumor sensitivity to FLASH radiotherapy. Int J Radiat Oncol 2024. https://doi.org/10.1016/j.ijrobp.2024.02.015.
[67] "Tumor hypoxia and radiotherapy: a major driver of resistance even for novel radiotherapy modalities," Semin Cancer Biol 2024;98:19–30, 10.1016/j.semcancer.2023.11.006.
[68] Alexander P. Division of biophysics: on the mode of action of some treatments that influence the radiation sensitivity of cells. Trans N Y Acad Sci 1962;24(8 Series II):966–78. https://doi.org/10.1111/j.2164-0947.1962.tb01456.x.
[69] Griffin RJ. International journal of radiation oncology, biology, physics. Int J Radiat Oncol Biol Phys 2006;66(2):627. https://doi.org/10.1016/j.ijrobp.2006.06.027.
[70] Delprat V, Huart C, Feron O, Soncin F, Michiels C. The impact of macrophages on endothelial cells is potentiated by cycling hypoxia: Enhanced tumor inflammation and metastasis. Front Oncol 2022;12. https://doi.org/10.3389/fonc.2022.961753.
[71] Michiels C, Tellier C, Feron O. Cycling hypoxia: a key feature of the tumor microenvironment. Biochim Biophys Acta BBA - Rev Cancer 2016;1866(1):76–86. https://doi.org/10.1016/j.bbcan.2016.06.004.
[72] Keith B, Johnson RS, Simon MC. HIF1α and HIF2α: sibling rivalry in hypoxic tumour growth and progression. Nat Rev Cancer 2012;12(1):9–22. https://doi.org/10.1038/nrc3183.
[73] Horsman MR, Overgaard J. The impact of hypoxia and its modification of the outcome of radiotherapy. J Radiat Res (Tokyo) 2016;57 Suppl 1(Suppl 1):i90–8. https://doi.org/10.1093/jrr/rrw007.
[74] Harada H. Hypoxia-inducible factor 1-mediated characteristic features of cancer cells for tumor radioresistance. J Radiat Res (Tokyo) 2016;57 Suppl 1(Suppl 1): i99–105. https://doi.org/10.1093/jrr/rrw012.
[75] Webb JD, Coleman ML, Pugh CW. Hypoxia, hypoxia-inducible factors (HIF), HIF hydroxylases and oxygen sensing. Cell Mol Life Sci 2009;66(22):3539–54. https://doi.org/10.1007/s00018-009-0147-7.
[76] Ling CC, Michaels HB, Epp ER, Peterson EC. Oxygen diffusion into mammalian cells following ultrahigh dose rate irradiation and lifetime estimates of oxygen-sensitive species. Radiat Res 1978;76(3):522–32. https://doi.org/10.2307/3574801.
[77] Dewey DL, Boag JW. Modification of the oxygen effect when bacteria are given large pulses of radiation. Nature 1959;183(4673):4673. https://doi.org/10.1038/1831450a0.
[78] Okoro CM, Schüler E, Taniguchi CM. The therapeutic potential of FLASH-RT for pancreatic cancer. Cancers 2022;14(5):5. https://doi.org/10.3390/cancers14051167.
[79] Wilson JD, Hammond EM, Higgins GS, Petersson K. Ultra-high dose rate (FLASH) radiotherapy: silver bullet or fool's gold? Front Oncol 2020;9. https://doi.org/10.3389/fonc.2019.01563.
[80] Hu A, Qiu R, Wu Z, Zhang H, Li WB, Li J. A computational model for oxygen depletion hypothesis in FLASH effect. Radiat Res 2021;197(2):175–83. https://doi.org/10.1667/RADE-20-00260.1.
[81] Boscolo D, Scifoni E, Durante M, Krämer M, Fuss MC. May oxygen depletion explain the FLASH effect? A chemical track structure analysis. Radiother Oncol 2021;162:68–75. https://doi.org/10.1016/j.radonc.2021.06.031.
[82] Jansen J, et al. Does FLASH deplete oxygen? Experimental evaluation for photons, protons, and carbon ions. Med Phys 2021;48(7):7. https://doi.org/10.1002/mp.14917.
[83] Jansen J, et al. Changes in Radical Levels as a Cause for the FLASH effect: Impact of beam structure parameters at ultra-high dose rates on oxygen depletion in water. Radiother Oncol 2022;175:193–6. https://doi.org/10.1016/j.radonc.2022.08.024.
[84] Khatib ME, et al. Ultrafast Tracking of oxygen dynamics during proton FLASH. Int J Radiat Oncol Biol Phys 2022;113(3):3. https://doi.org/10.1016/j.ijrobp.2022.03.016.
[85] Slyke ALV, et al. Oxygen monitoring in model solutions and in vivo in mice during proton irradiation at conventional and FLASH dose rates. Radiat Res 2022; 198(2):2. https://doi.org/10.1667/RADE-21-00232.1.
[86] Cao X, et al. Quantification of oxygen depletion during FLASH irradiation in vitro and in vivo. Int J Radiat Oncol Biol Phys 2021;111(1). https://doi.org/10.1016/j.ijrobp.2021.03.056.
[87] Sunnerberg JP, Zhang R, Gladstone DJ, Swartz HM, Gui J, Pogue BW. Mean dose rate in ultra-high dose rate electron irradiation is a significant predictor for O_2 consumption and H_2O_2 yield. Phys Med Biol 2023;68(16):16. https://doi.org/10.1088/1361-6560/ace877.
[88] Koch CJ, Kim MM, Wiersma RD. Radiation-chemical oxygen depletion depends on chemical environment and dose rate: implications for the FLASH effect. Int J Radiat Oncol Biol Phys 2023;117(1):1. https://doi.org/10.1016/j.ijrobp.2023.04.001.
[89] Cooper CR, Jones D, Jones GD, Petersson K. FLASH irradiation induces lower levels of DNA damage ex vivo, an effect modulated by oxygen tension, dose, and dose rate. Br J Radiol 2022;95(1133):20211150. https://doi.org/10.1259/bjr.20211150.
[90] Ohsawa D, et al. DNA strand break induction of aqueous plasmid DNA exposed to 30 MeV protons at ultra-high dose rate. J Radiat Res (Tokyo) 2022;63(2):255–60. https://doi.org/10.1093/jrr/rrab114.
[91] Small KL, et al. Evaluating very high energy electron RBE from nanodosimetric pBR322 plasmid DNA damage. Sci Rep 2021;11(1):1. https://doi.org/10.1038/s41598-021-82772-6.
[92] Konishi T, Kusumoto T, Hiroyama Y, Kobayashi A, Mamiya T, Kodaira S. Induction of DNA strand breaks and oxidative base damages in plasmid DNA by ultra-high dose rate proton irradiation. Int J Radiat Biol 2023;99(9):1405–12. https://doi.org/10.1080/09553002.2023.2176562.

[93] Schmitt F-J, et al. Reactive oxygen species: Re-evaluation of generation, monitoring and role in stress-signaling in phototrophic organisms. Biochim Biophys Acta BBA - Bioenerg 2014;1837(6):835–48. https://doi.org/10.1016/j.bbabio.2014.02.005.

[94] Thompson SJ, Prise KM, McMahon SJ. Investigating the potential contribution of inter-track interactions within ultra-high dose-rate proton therapy. Phys Med Biol 2023;68(5):055006. https://doi.org/10.1088/1361-6560/acb88a.

[95] Alanazi A, Meesungnoen J, Jay-Gerin J-P. A computer modeling study of water radiolysis at high dose rates. Relevance to FLASH radiotherapy. Radiat Res 2021;195(2):149–62. https://doi.org/10.1667/RADE-20-00168.1.

[96] Kreipl MS, Friedland W, Paretzke HG. Interaction of ion tracks in spatial and temporal proximity. Radiat Environ Biophys 2009;48(4):349–59. https://doi.org/10.1007/s00411-009-0234-z.

[97] Abolfath R, Grosshans D, Mohan R. Oxygen depletion in FLASH ultra-high-dose-rate radiotherapy: a molecular dynamics simulation. Med Phys 2020;47(12):6551–61. https://doi.org/10.1002/mp.14548.

[98] Khalifa J, et al. Gene therapy and cell therapy for the management of radiation damages to healthy tissues: rationale and early results. Cancer/Radiothérapie 2019;23(5):449–65. https://doi.org/10.1016/j.canrad.2019.06.002.

[99] Kim Y-E, et al. Effects of UltRA-HIGH doserate FLASH irradiation on the tumor microenvironment in lewis lung carcinoma: role of myosin light chain. Int J Radiat Oncol 2021;109(5):1440–53. https://doi.org/10.1016/j.ijrobp.2020.11.012.

[100] Murphy MP, et al. Guidelines for measuring reactive oxygen species and oxidative damage in cells and in vivo. Nat Metab 2022;4(6):6. https://doi.org/10.1038/s42255-022-00591-z.

[101] Blain G, et al. Proton irradiations at ultra-high dose rate vs. conventional dose rate: strong impact on hydrogen peroxide yield. Radiat Res 2022;198(3):318–24. https://doi.org/10.1667/RADE-22-00021.1.

[102] Kacem H, et al. Comparing radiolytic production of H_2O_2 and development of Zebrafish embryos after ultra high dose rate exposure with electron and transmission proton beams. Radiother Oncol 2022;175:197–202. https://doi.org/10.1016/j.radonc.2022.07.011.

[103] Thomas W, et al. Proton and electron ultrahigh-dose-rate isodose irradiations produce differences in reactive oxygen species yields. Int J Radiat Oncol 2023. https://doi.org/10.1016/j.ijrobp.2023.07.042.

[104] Froidevaux P, Grilj V, Bailat C, Geyer WR, Bochud F, Vozenin M-C. FLASH irradiation does not induce lipid peroxidation in lipids micelles and liposomes. Radiat Phys Chem 2023;205:110733. https://doi.org/10.1016/j.radphyschem.2022.110733.

[105] Hunyor I, Cook KM. Models of intermittent hypoxia and obstructive sleep apnea: molecular pathways and their contribution to cancer. Am J Physiol-Regul Integr Comp Physiol 2018;315(4):R669–87. https://doi.org/10.1152/ajpregu.00036.2018.

[106] Ortiz-Prado E, Dunn JF, Vasconez J, Castillo D, Viscor G. Partial pressure of oxygen in the human body: a general review. Am J Blood Res 2019;9(1):1–14.

[107] Vaupel P, et al. From localized mild hyperthermia to improved tumor oxygenation: physiological mechanisms critically involved in oncologic thermo-radio-immunotherapy. Cancers 2023;15(5):1394. https://doi.org/10.3390/cancers15051394.

[108] Moen I, Stuhr LEB. Hyperbaric oxygen therapy and cancer—a review. Target Oncol 2012;7(4):233–42. https://doi.org/10.1007/s11523-012-0233-x.

[109] Spitz DR, et al. An integrated physico-chemical approach for explaining the differential impact of FLASH versus conventional dose rate irradiation on cancer and normal tissue responses. Radiother Oncol J Eur Soc Ther Radiol Oncol 2019;139:23–7. https://doi.org/10.1016/j.radonc.2019.03.028.

[110] Labarbe R, Hotoiu L, Barbier J, Favaudon V. A physicochemical model of reaction kinetics supports peroxyl radical recombination as the main determinant of the FLASH effect. Radiother Oncol 2020;153:303–10. https://doi.org/10.1016/j.radonc.2020.06.001.

[111] Hu A, et al. Radical recombination and antioxidants: a hypothesis on the FLASH effect mechanism. Int J Radiat Biol 2023;99(4):4. https://doi.org/10.1080/09553002.2022.2110307.

[112] Kehm R, Baldensperger T, Raupbach J, Höhn A. Protein oxidation - Formation mechanisms, detection and relevance as biomarkers in human diseases. Redox Biol 2021;42:101901. https://doi.org/10.1016/j.redox.2021.101901.

[113] Schöneich C, Sharov VS. Mass spectrometry of protein modifications by reactive oxygen and nitrogen species. Free Radic Biol Med 2006;41(10):1507–20. https://doi.org/10.1016/j.freeradbiomed.2006.08.013.

[114] Wardman P. Approaches to modeling chemical reaction pathways in radiobiology. Int J Radiat Biol 2022;98(9):1399–413. https://doi.org/10.1080/09553002.2022.2033342.

[115] Van de Bittner GC, Dubikovskaya EA, Bertozzi CR, Chang CJ. In vivo imaging of hydrogen peroxide production in a murine tumor model with a chemoselective bioluminescent reporter. Proc Natl Acad Sci u s a 2010;107(50):21316–21. https://doi.org/10.1073/pnas.1012864107.

[116] Zielonka J, Podsiadły R, Zielonka M, Hardy M, Kalyanaraman B. On the use of peroxy-caged luciferin (PCL-1) probe for bioluminescent detection of inflammatory oxidants in vitro and in vivo - Identification of reaction intermediates and oxidant-specific minor products. Free Radic Biol Med 2016;99:32–42. https://doi.org/10.1016/j.freeradbiomed.2016.07.023.

[117] Ma Q, et al. A new bioluminescent imaging technology for studying oxidative stress in the testis and its impacts on fertility. Free Radic Biol Med 2018;124:51–60. https://doi.org/10.1016/j.freeradbiomed.2018.05.080.

[118] Lameka K, Farwell MD, Ichise M. Positron emission tomography. Handb Clin Neurol 2016;135:209–27. https://doi.org/10.1016/B978-0-444-53485-9.00011-8.

[119] Boutagy NE, et al. In Vivo reactive oxygen species detection with a novel positron emission tomography tracer, 18F-DHMT, allows for early detection of anthracycline-induced cardiotoxicity in rodents. JACC Basic Transl Sci 2018;3(3):378–90. https://doi.org/10.1016/j.jacbts.2018.02.003.

[120] Chu W, et al. Development of a PET radiotracer for non-invasive imaging of the reactive oxygen species, superoxide, in vivo. Org Biomol Chem 2014;12(25):4421–31. https://doi.org/10.1039/c3ob42379d.

[121] "18F-Labeled dihydromethidine: positron emission tomography radiotracer for imaging of reactive oxygen species in intact brain," *Org Biomol Chem* 2020;18(13):2387–91, 10.1039/d0ob00126k.

[122] Sivapackiam J, et al. Galuminox: preclinical validation of a novel PET tracer for non-invasive imaging of oxidative stress in vivo. Redox Biol 2020;37:101690. https://doi.org/10.1016/j.redox.2020.101690.

[123] Yu X, Ouyang W, Qiu H, Zhang Z, Wang Z, Xing B. Detection of reactive oxygen and nitrogen species by upconversion nanoparticle-based near-infrared nanoprobes: recent progress and perspectives. Chem – Eur J 2022;28(65):e202201966.

[124] Li Z, Liang T, Lv S, Zhuang Q, Liu Z. A rationally designed upconversion nanoprobe for in vivo detection of hydroxyl radical. J Am Chem Soc 2015;137(34):11179–85. https://doi.org/10.1021/jacs.5b06972.

[125] Hao C, et al. Chiral Core-shell upconversion nanoparticle@MOF nanoassemblies for quantification and bioimaging of reactive oxygen species in vivo. J Am Chem Soc 2019;141(49):19373–8. https://doi.org/10.1021/jacs.9b09360.

[126] Wang H, Li Y, Yang M, Wang P, Gu Y. FRET-based upconversion nanoprobe sensitized by Nd^{3+} for the ratiometric detection of hydrogen peroxide in vivo. ACS Appl Mater Interfaces 2019;11(7):7441–9. https://doi.org/10.1021/acsami.8b21549.

[127] Yang W, et al. Novel near-infrared fluorescence probe for bioimaging and evaluating superoxide anion fluctuations in ferroptosis-mediated epilepsy. Anal Chem 2023;95(33):12240–6. https://doi.org/10.1021/acs.analchem.3c00852.

[128] Halliwell B, Whiteman M. Measuring reactive species and oxidative damage in vivo and in cell culture: how should you do it and what do the results mean? Br J Pharmacol 2004;142(2):231–55. https://doi.org/10.1038/sj.bjp.0705776.

[129] Huycke MM, Moore DR. In vivo production of hydroxyl radical by Enterococcus faecalis colonizing the intestinal tract using aromatic hydroxylation. Free Radic Biol Med 2002;33(6):818–26. https://doi.org/10.1016/s0891-5849(02)00977-2.

[130] Mishin VM, Thomas PE. Characterization of hydroxyl radical formation by microsomal enzymes using a water-soluble trap, terephthalate. Biochem Pharmacol 2004;68(4):747–52. https://doi.org/10.1016/j.bcp.2004.05.004.

[131] Setsukinai K, Urano Y, Kakinuma K, Majima HJ, Nagano T. Development of novel fluorescence probes that can reliably detect reactive oxygen species and distinguish specific species*210. J Biol Chem 2003;278(5):3170–5. https://doi.org/10.1074/jbc.M209264200.

[132] Kostyuk AI, et al. In Vivo Imaging with Genetically Encoded Redox Biosensors. Int J Mol Sci 2020;21(21):21. https://doi.org/10.3390/ijms21218164.

[133] Czowski BJ, Romero-Moreno R, Trull KJ, White KA. Cancer and pH dynamics: transcriptional regulation, proteostasis, and the need for new molecular tools. Cancers 2020;12(10):10. https://doi.org/10.3390/cancers12102760.

[134] White KA, Grillo-Hill BK, Barber DL. Cancer cell behaviors mediated by dysregulated pH dynamics at a glance. J Cell Sci 2017;130(4):663–9. https://doi.org/10.1242/jcs.195297.

[135] Dopp IJ, Kalac K, Mackenzie SA. Hydrogen peroxide sensor HyPer7 illuminates tissue-specific plastid redox dynamics. Plant Physiol 2023;193(1):217–28. https://doi.org/10.1093/plphys/kiad307.

[136] Morgan B, et al. Real-time monitoring of basal H_2O_2 levels with peroxiredoxin-based probes. Nat Chem Biol 2016;12(6):437–43. https://doi.org/10.1038/nchembio.2067.

[137] Panieri E, Santoro MM. Data on metabolic-dependent antioxidant response in the cardiovascular tissues of living zebrafish under stress conditions. Data Brief 2017;12:427–32. https://doi.org/10.1016/j.dib.2017.04.034.

[138] Panieri E, Millia C, Santoro MM. Real-time quantification of subcellular H2O2 and glutathione redox potential in living cardiovascular tissues. Free Radic Biol Med 2017;109:189–200. https://doi.org/10.1016/j.freeradbiomed.2017.02.022.

[139] Müller A, Schneider JF, Degrossoli A, Lupilova N, Dick TP, Leichert LI. Systematic in vitro assessment of responses of roGFP2-based probes to physiologically relevant oxidant species. Free Radic Biol Med 2017;106:329–38. https://doi.org/10.1016/j.freeradbiomed.2017.02.044.

[140] Smolyarova DD, Podgorny OV, Bilan DS, Belousov VV. A guide to genetically encoded tools for the study of H_2O_2. FEBS J 2022;289(18):5382–95. https://doi.org/10.1111/febs.16088.

[141] Portier L, et al. Differential remodeling of the oxylipin pool after FLASH versus conventional dose-rate irradiation in vitro and in vivo. Int J Radiat Oncol 2024. https://doi.org/10.1016/j.ijrobp.2024.01.210.

[142] Dayal D, et al. Mitochondrial complex II dysfunction can contribute significantly to genomic instability after exposure to ionizing radiation. Radiat Res 2009;172(6):737–45. https://doi.org/10.1667/RR1617.1.

[143] Dayal D, Martin SM, Limoli CL, Spitz DR. Hydrogen peroxide mediates the radiation-induced mutator phenotype in mammalian cells. Biochem J 2008;413(1):185–91. https://doi.org/10.1042/BJ20071643.

[144] Zielonka J, et al. Mitochondria-targeted triphenylphosphonium-based compounds: syntheses, mechanisms of action, and therapeutic and diagnostic applications. Chem Rev 2017;117(15):10043–120. https://doi.org/10.1021/acs.chemrev.7b00042.

[145] Kagan VE, Chu CT, Tyurina YY, Cheikhi A, Bayir H. Cardiolipin asymmetry, oxidation and signaling. Chem Phys Lipids 2014;179:64–9. https://doi.org/10.1016/j.chemphyslip.2013.11.010.
[146] Kagan VE, et al. Cytochrome c acts as a cardiolipin oxygenase required for release of proapoptotic factors. Nat Chem Biol 2005;1(4):4. https://doi.org/10.1038/nchembio727.
[147] Dixon SJ, et al. Ferroptosis: an iron-dependent form of nonapoptotic cell death. Cell 2012;149(5):1060–72. https://doi.org/10.1016/j.cell.2012.03.042.
[148] Li J, et al. Ferroptosis: past, present and future. Cell Death Dis 2020;11(2):2. https://doi.org/10.1038/s41419-020-2298-2.
[149] Su J, et al. Cooperation effects of radiation and ferroptosis on tumor suppression and radiation injury. Front Cell Dev Biol 2022;10:951116. https://doi.org/10.3389/fcell.2022.951116.
[150] Lang X, et al. Radiotherapy and immunotherapy promote tumoral lipid oxidation and ferroptosis via synergistic repression of SLC7A11. Cancer Discov 2019;9(12):1673–85. https://doi.org/10.1158/2159-8290.CD-19-0338.
[151] Ye LF, et al. Radiation-induced lipid peroxidation triggers ferroptosis and synergizes with ferroptosis inducers. ACS Chem Biol 2020;15(2):469–84. https://doi.org/10.1021/acschembio.9b00939.
[152] Lei G, et al. The role of ferroptosis in ionizing radiation-induced cell death and tumor suppression. Cell Res 2020;30(2):2. https://doi.org/10.1038/s41422-019-0263-3.
[153] Kale RK, Sitasawad SL. Radiation induced lipid peroxidation in liposomes. Int J Radiat Appl Instrum Part C Radiat Phys Chem 1990;36(3):361–4. https://doi.org/10.1016/1359-0197(90)90019-E.
[154] Petkau A, Chelack WS. Radioprotective effect of superoxide dismutase on model phospholipid membranes. Biochim Biophys Acta BBA - Biomembr 1976;433(3):445–56. https://doi.org/10.1016/0005-2736(76)90272-8.
[155] Raleigh JA, Kremers W, Gaboury B. Dose-rate and oxygen effects in models of lipid membranes: linoleic acid. Int J Radiat Biol Relat Stud Phys Chem Med 1977;31(3):203–13. https://doi.org/10.1080/09553007714550251.
[156] Yukawa O, Nakazawa T. Radiation-induced lipid peroxidation and membrane-bound enzymes in liver microsomes. Int J Radiat Biol Relat Stud Phys Chem Med 1980;37(5):621–31. https://doi.org/10.1080/09553008014550781.
[157] Stark G. The effect of ionizing radiation on lipid membranes. Biochim Biophys Acta BBA - Rev Biomembr 1991;1071(2):103–22. https://doi.org/10.1016/0304-4157(91)90020-W.
[158] Zhu H, et al. Radioprotective effect of X-ray abdominal FLASH irradiation: adaptation to oxidative damage and inflammatory response may be benefiting factors. Med Phys 2022;49(7):4812–22. https://doi.org/10.1002/mp.15680.
[159] Vilaplana-Lopera N, Abu-Halawa A, Walker E, Kim J, Moon EJ. Ferroptosis, a key to unravel the enigma of the FLASH effect? Br J Radiol 2022;95(1140):20220825. https://doi.org/10.1259/bjr.20220825.
[160] Jung M, Mertens C, Tomat E, Brüne B. Iron as a central player and promising target in cancer progression. Int J Mol Sci 2019;20. https://doi.org/10.3390/ijms20020273.
[161] Sun H, Zhang C, Cao S, Sheng T, Dong N, Xu Y. Fenton reactions drive nucleotide and ATP syntheses in cancer. J Mol Cell Biol 2018;10(5):448–59. https://doi.org/10.1093/jmcb/mjy039.
[162] Torti SV, Torti FM. Iron and cancer: more ore to be mined. Nat Rev Cancer 2013;13(5):5. https://doi.org/10.1038/nrc3495.
[163] Zhang C, Zhang F. Iron homeostasis and tumorigenesis: molecular mechanisms and therapeutic opportunities. Protein Cell 2015;6(2):88–100. https://doi.org/10.1007/s13238-014-0119-z.
[164] Luanpitpong S, et al. Regulation of lung cancer cell migration and invasion by reactive oxygen species and caveolin-1 *. J Biol Chem 2010;285(50):38832–40. https://doi.org/10.1074/jbc.M110.124958.
[165] Kim D-H, et al. 15-Deoxy-Δ 12,14 -prostaglandin J 2 upregulates the expression of heme oxygenase-1 and subsequently matrix metalloproteinase-1 in human breast cancer cells: possible roles of iron and ROS. Carcinogenesis 2009;30(4):645–54. https://doi.org/10.1093/carcin/bgp012.
[166] Citrin DE, Mitchell JB. Mechanisms of normal tissue injury from irradiation. Semin Radiat Oncol 2017;27(4):316–24. https://doi.org/10.1016/j.semradonc.2017.04.001.
[167] Nguyen HQ, et al. Ionizing radiation-induced cellular senescence promotes tissue fibrosis after radiotherapy. A review. Crit Rev Oncol Hematol 2018;129:13–26. https://doi.org/10.1016/j.critrevonc.2018.06.012.
[168] Kim JH, Brown SL, Gordon MN. Radiation-induced senescence: therapeutic opportunities. Radiat Oncol Lond Engl 2023;18(1):10. https://doi.org/10.1186/s13014-022-02184-2.
[169] Fouillade C, et al. FLASH irradiation spares lung progenitor cells and limits the incidence of radio-induced senescence. Clin Cancer Res 2020;26(6):6. https://doi.org/10.1158/1078-0432.CCR-19-1440.
[170] Huang W, Hickson LJ, Eirin A, Kirkland JL, Lerman LO. Cellular senescence: the good, the bad and the unknown. Nat Rev Nephrol 2022;18(10):611–27. https://doi.org/10.1038/s41581-022-00601-z.
[171] Lu T, Finkel T. Free Radicals and Senescence. Exp Cell Res 2008;314(9):1918–22. https://doi.org/10.1016/j.yexcr.2008.01.011.
[172] Lin JB, et al. Macrophage microRNA-150 promotes pathological angiogenesis as seen in age-related macular degeneration. JCI Insight 2018;3(7). https://doi.org/10.1172/jci.insight.120157.
[173] Hernandez-Segura A, Nehme J, Demaria M. Hallmarks of cellular senescence. Trends Cell Biol 2018;28(6):436–53. https://doi.org/10.1016/j.tcb.2018.02.001.
[174] Blaser H, Dostert C, Mak TW, Brenner D. TNF and ROS crosstalk in inflammation. Trends Cell Biol 2016;26(4):249–61. https://doi.org/10.1016/j.tcb.2015.12.002.